Climatology of Warm Rain and Associated Latent Heating Derived from TRMM PR Observations

YASU-MASA KODAMA

Department of Earth and Environmental Sciences, Graduate School of Science and Technology, Hirosaki University, Hirosaki, Aomori, Japan

MASAKI KATSUMATA AND SHUICHI MORI

Institute of Observational Research for Global Change, Japan Agency for Marine-Earth Science and Technology, Yokosuka, Kanagawa, Japan

SINSUKE SATOH

Applied Electromagnetic Research Center, National Institute of Information and Communications Technology, Koganei, Tokyo, Japan

YUKI HIROSE AND HIROAKI UEDA

Division of Geoenvironmental Sciences, Graduate School of Life and Environmental Sciences, University of Tsukuba, Tsukuba, Ibaraki, Japan

(Manuscript received 11 April 2008, in final form 8 April 2009)

ABSTRACT

The large-scale distribution of precipitation and latent heating (LH) profiles in the tropics, subtropics, and part of the midlatitudes was studied using a 9-yr dataset derived from Tropical Rainfall Measuring Mission precipitation radar observations, with emphasis on the contribution of warm rain. The distribution of warm rain showed features unique from those of rain in other categories and those of outgoing longwave radiation. Warm rain was weak over land but widely distributed over oceans, especially along the intertropical convergence zone (ITCZ) and the western part of the subtropical oceans. The observed amount of warm rain depended on the rainfall intensity rather than on the frequency of warm rain events. The amount of warm rain over ocean was positively correlated with sea surface temperature (SST); this dependency was found in the tropics, subtropics, and part of the midlatitudes, whereas dependency of SST on total rain was confined to the tropics. Both total rain and warm rain were concentrated in the ITCZ, which elongated along the local SST maximum. Small amounts of warm rain were found along subtropical convergence zones (the baiu frontal zone and subtropical portions of the South Pacific convergence zone and the South Atlantic convergence zone) with ample total rainfall. However, larger amounts of warm rain were observed at the lower-latitude sides of these zones in the upstream portions of low-level moisture flow toward the zones. Warm rain may cultivate the subtropical convergence zones by deepening the moist boundary layer and increasing moisture flux toward the zones. The statistical relationship between warm rain and low-level cloudiness showed that the warm rain amount was large when low-level cloudiness was 20%–30% and small when low-level cloudiness was greater than 40%. This indicates that intense warm rain is provided by convective clouds, not by stratiform clouds, in conditions of substantial cloudiness. Despite the small contribution to total rain, warm rain maintained positive LH values over most of the tropical and subtropical oceans. The LH by warm rain masked low-level cooling observed in stratiform rain and maintained positive LH in the lower atmosphere below the melting layer. Because warm rain was confined to oceans, a strong LH contrast was maintained along the coast; this contrast reached values of 1–2 K day^{-1} in certain places and may affect local and monsoonal circulation across continental coasts.

Corresponding author address: Yasu-Masa Kodama, Department of Earth and Environmental Sciences, Hirosaki University, Hirosaki, Aomori 036-8561, Japan.
E-mail: kodama@cc.hirosaki-u.ac.jp

DOI: 10.1175/2009JCLI2575.1

1. Introduction

The global distribution of precipitation is related to water circulation in the climate system and to latent heating (LH) in the atmosphere, which is an important heat source driving atmospheric circulation (Nigam et al. 2000). Characteristics of precipitation change greatly over a wide spectrum according to precipitation type and surface and atmospheric conditions. Satellite observations of clouds have provided useful but indirect information on precipitation. Precipitation from low-level clouds is especially difficult to evaluate because upper clouds disturb the observation of low-level clouds from space. Observation by satellite-borne precipitation radar (PR) began with the launch of the Tropical Rainfall Measuring Mission (TRMM) satellite in late 1997. The PR instrument on TRMM (TRMM PR) can observe the vertical structure of precipitation, including precipitation from low-level clouds. Heat and moisture budget analyses have been conducted to evaluate the contribution of LH to the large-scale distribution of atmospheric heat sources (e.g., Yanai et al. 1973; Luo and Yanai 1984; Lin and Johnson 1996; Schumacher et al. 2007). Information on the large-scale distribution of LH profiles is also expected from TRMM PR observations (Simpson et al. 1988) because the precipitation profiles observed by PR are closely related to LH profiles, which cannot be remotely sensed by satellite instruments in a straightforward way. Several algorithms have been proposed for obtaining LH profiles indirectly from TRMM PR observations, and discrepancies among the results of such algorithms are not significant (Tao et al. 2006).

The first objective of this study is a climatic description of warm rain in the tropics, subtropics, and part of the midlatitudes. Warm rain is defined as originating from clouds that are entirely warmer than freezing (Beard and Ochs 1993). The contribution of warm rain to precipitation and LH is not negligible. Johnson et al. (1999) proposed trimodal characteristics of convection over tropical oceans, with shallow cumulus below trade inversions, congestus clouds with tops near the 0°C level, and cumulonimbus with tops near the tropopause. A stable layer near the 0°C level, maintained by the LH of melting snow (Johnson et al. 1996), allows for the formation of congestus, which provides strong rainfall. In the subtropical oceans, congestus along with shallow cumulus mix the atmospheric boundary layer and the free troposphere and affect the intertropical convergence zone (ITCZ) by modifying the moisture and temperature stratification of the air flowing into the ITCZ (Neggers et al. 2007).

The majority of rainfall from congestus is warm rain because the tops of most congestus are near the 0°C level and considered not to be frozen. Johnson et al. (1999) also showed that the number of shallow cumulus and congestus clouds was correlated positively with sea surface temperature (SST) during the two cruises of the R/V *Vickers* in the intensive observation period (IOP) of the Tropical Ocean and Global Atmosphere Coupled Ocean–Atmosphere Response Experiment (TOGA COARE). Schumacher et al. (2007) noted that low-level (~750 hPa) heating and mid- and upper-level cooling were frequently observed in Q1 atmospheric heat source profiles in the ITCZ over the central Pacific. Cooling was evaluated by heat and moisture budget analyses using aerological data from the Kwajalein Experiment. The low-level heating was maintained by LH in cumulus, which developed into the midtroposphere, whereas mid- and upper-level cooling corresponded to detrainment and radiative cooling. This strongly suggests that cumulus congestus forms the low-level positive peak of LH observed in the ITCZ (Schumacher et al. 2007; Thompson et al. 1979). However, despite growing interest in warm rain, our knowledge of the global-scale distribution of warm rain remains poor. Lau and Wu (2003) demonstrated a significant contribution of warm rain to total rain in amount and areal coverage. However, they analyzed data derived from passive microwave observations of the TRMM, and the distinction of warm rain from deep rain was not critical. The TRMM PR is preferable for detecting warm rain because the PR can classify precipitation by echo-top height. Recently, the version 6 data product of TRMM PR was released. It provides a detailed index of precipitation features by which we can evaluate the contribution of warm rain (TRMM Precipitation Radar Team 2005). The climatic distribution of warm rain and its relationship to the land–sea distribution, SST, low-level cloudiness, and low-level circulation are examined in this study.

Another objective is to describe the large-scale distribution of LH profiles, with an emphasis on the contribution of warm rain. Latent heat is the major driving force of atmospheric circulation in the tropics and the subtropics. To evaluate LH profiles, the PR heating (PRH) algorithm is implemented in this study. The retrieval method used to obtain LH from radar reflectivity profiles was originally developed by Satoh and Noda (2001) and Satoh (2004) and revised by Katsumata (2007). The algorithm is described briefly in the appendix.

The remainder of this section reviews previous studies on warm rain. Coalescence is the essential process of warm rain and becomes effective when clouds include large droplets of more than 30–50 μm; smaller droplets cannot capture other smaller droplets efficiently for aerodynamic reasons (Klett and Davis 1973; Beard and Ochs 1993). Beard and Ochs (1984, 1993) also reported

that a lower density of cloud condensation nuclei (CCN) is favorable for generating large cloud droplets by condensation processes. This means that warm rain is more likely to occur over oceans than over continents because the density of CCN is much lower over the ocean. Houze (1993, chapter 6) has noted that updraft intensifies cloud coalescence processes. This is because raindrops sustained by convective updrafts can capture more cloud droplets than can raindrops in stratiform clouds. Ogura and Takahashi (1973) and Takahashi (1981) demonstrated warm-rain development in maritime shallow convective clouds by numerical experiments. By a large-eddy simulation that incorporated a size-resolving representation, Stevens et al. (1998) showed that shallow stratocumulus cannot persist in the presence of strong precipitation. Precipitation cools and moistens the subcloud layer and favors the formation of cumulus, not stratocumulus. Our study on the behavior of warm rain may provide observational evidence supporting these previous studies because few similar studies have examined large-scale fields of warm rain.

By analyzing TRMM PR data, Short and Nakamura (2000) found that a double-decked structure peaked at approximately 2 and 5 km above mean sea level (MSL) in echo-top-height histograms over oceans. The lower deck located at ~2 km MSL corresponded to maritime stratocumulus clouds and was widely distributed mainly over ocean. Note that warm rain in this study includes cumulus congestus, which was not included in the shallow rain measurements of Short and Nakamura (2000).

We must also consider the limitations of TRMM PR for shallow rain observation. Short and Nakamura (2000) pointed out that the intensity of shallow rain may be underestimated because of insufficient radar sensitivity to weak rain or drizzle and surface-clutter contamination in shallow rain. Cifelli et al. (2007) analyzed precipitation systems over the ITCZ in the eastern Pacific off Central America (10°N, 95°W) using TRMM PR and shipborne radar data obtained during the Eastern Pacific Investigation of Climate Processes in the Coupled Ocean–Atmosphere System (EPIC) campaign. They found that a large number of small (less than 100 km^2) and shallow rain events below the dry layer around 800 hPa were observed. Part of the weak and small shallow rain observed by the ship-based radar was not captured by TRMM PR because of the higher threshold of reflectivity and lower horizontal resolution (4.3 and 5.0 km before and after the reboost of TRMM in 2001, respectively), which caused partial beam filling of convective clouds in TRMM PR pixels. These features of the TRMM PR may lead to the underestimation of small rainfall clouds, which may be dominant over land (T. Iguchi 2007, personal communication). Ground clutter disturbs shallow rain observations, especially near the edge of PR scans, and may cause the underestimation of shallow rain with tops below the bottom of TRMM PR observations. This effect may be more severe over oceans, where shallow rain is dominant, than over land (M. Hirose 2007, personal communication). The reboost of TRMM in August 2001 may have some influence on the rainfall intensity in the resulting TRMM PR product, especially in regard to missed observations of weak rain (Nakazawa and Rajendran 2009; DeMoss and Bowman 2007). Part of warm rain, along with accompanying LH, may be weakly evaluated because of the reboost. Nakazawa and Rajendran (2009) pointed out that the frequency of weak rain in TRMM observations significantly decreased after the reboost. However, we do not consider possible changes caused by the reboost because year-to-year variation is not treated. The following section describes the algorithms used in this study to evaluate LH. Section 3 presents the data, and sections 4 and 5 discuss the precipitation and LH, respectively, focusing on the contribution of warm rain. Finally, we summarize our study and propose future research tasks in section 6.

2. Algorithms for estimating LH

LH is the primary heat source in the tropical and subtropical atmosphere. To describe atmospheric heat sources and the contribution of LH, Yanai et al. (1973) proposed a formulation involving Q1 and Q2, which are residuals of heat and moisture budgets of the resolvable motion, respectively. Each can be interpreted as

$$\mathrm{Q1} = Q_R + \mathrm{LH} - \frac{\partial}{\partial p}\overline{s'\omega'}, \tag{1}$$

$$\mathrm{Q2} = \mathrm{LH} + L\frac{\partial}{\partial p}\partial\overline{q'\omega'}, \tag{2}$$

$$\mathrm{LH} = L(c - e), \tag{3}$$

where $s \equiv C_pT + gz$ is the dry static energy, and L, c, e, q, ω, and Q_R are the specific latent heat, condensation rate, evaporation rate, mixing ratio of humidity, vertical p velocity, and radiative heating rate, respectively. Primed variables are anomalies from the horizontal average, corresponding to convective-scale variations. Q1 represents the atmospheric heat source, and Q2 represents the moisture sink. LH is the major part of Q1 in a rainfall area. Vertical profiles agree between Q1 and LH for stratiform rain. However, a positive peak in Q1 shifts higher than the LH peak for convective rain because of convective upward transport of sensible heat from the level of maximum condensation as detected by the maximum LH (Luo and Yanai 1984).

TABLE 1. Correspondence between the rain type by the version 6 2A25 product and the PRH algorithm.

Rain type by the PRH algorithm	Storm height (stmht)	Rain type by the version 6 2A25 product
Warm (shallow)	below ML	152 (stratiform, shallow), 251–291 (convective, shallow), 312 (other shallow)
Convective	above ML	200–240 (convective)
Stratiform	above ML	100–140 (stratiform)
Anvil	above ML	160, 170 (stratiform, no rain near surface), 300, 313 (other, shallow)

Q1 is adequate for describing the atmospheric heat source maintaining large-scale atmospheric circulation. However, LH should be described by TRMM PR observations (Simpson et al. 1988) because TRMM PR cannot observe radiative heating and heat transport by convective processes. Although processes of positive LH (i.e., moisture condensation on cloud droplets) cannot be observed by PR, two algorithms using TRMM PR data have been proposed to bypass this problem: one is a PRH algorithm (Satoh and Noda 2001; Satoh 2004), and the other is a spectral latent heating (SLH) algorithm (Shige et al. 2004, 2007). The SLH algorithm evaluates LH profiles using lookup tables, prepared by simulations of a cloud-resolving model (CRM), whereas the PRH algorithm is a retrieval method to evaluate the LH profile from the profile of radar reflectivity. The merits and demerits of these algorithms were discussed by Tao et al. (2006). We adopted an improved version of the PRH algorithm released by Katsumata (2007). A brief description of the improved version is shown in the appendix.

In the PRH algorithm, rainfall is classified into four types (convective, stratiform, shallow, and anvil, as shown in Table 1) using the version 6 algorithms of the 2A25 product of TRMM (TRMM Precipitation Radar Team 2005). Here, anvil rain is defined as rain that evaporates before reaching the surface. Shallow rain is defined as having a detectable echo top (more than ~18 dBZ) lower than the melting level (ML). Hereafter, shallow rain is referred to as warm rain. Some problems may occur with our definition of warm rain. For example, rain influenced by ice provided by upper ice-phase clouds undetectable by PR cannot be excluded from the warm rain type, whereas warm rain covered by upper-level anvil clouds with a detectable echo but with no influence of ice is not classified as warm rain. Later, we will compare the frequencies of warm rain and upper-tropospheric echoes to show that the latter problem is not serious.

3. Data

We used climatological data of precipitation and LH profiles for nine years between 1998 and 2006. These data were prepared by applying the version 6.4 PRH algorithms (Katsumata 2007) to version 6 2A25 products of TRMM PR observations. The climatological data included near-surface rain and profiles of precipitation and LH at 2.5° × 2.5° grid squares and vertically at 500-m intervals between 35°S and 35°N. We defined near-surface rain as rain intensity at the lowest height of clutter-free observation. The height changes between approximately 500 m from the surface at nadir and 2000 m at the edge of the swath. The precipitation and accompanying LH were classified into four rain types (stratiform, convective, anvil, and warm) determined for each 4.3- or 5.0-km-square pixel of TRMM PR, following the classification by the version 6.4 PRH algorithm. Table 1 shows the correspondence of rainfall classification between the version 6.4 PRH and version 6 2A25 algorithms. Monthly averaged National Centers for Environmental Prediction–National Center for Atmospheric Research (NCEP–NCAR) reanalysis, outgoing longwave radiation (OLR) data [National Oceanic and Atmospheric Administration (NOAA) interpolated OLR; Liebmann and Smith 1996], SST data [NOAA optimal interpolation (OI), version 2, monthly SST analysis; Reynolds et al. 2002], and cloudiness data [International Satellite Cloud Climatology Project (ISCCP) D2 monthly cloudiness data (ISCCP-D2; Schiffer and Rossow 1983; Rossow and Schiffer 1999)] were used for reference.

4. Precipitation

Figure 1 shows 9-yr averaged near-surface rain in four months (January, April, July, and October) representing different seasons. The figure also shows the composition of near-surface rain (i.e., convective, stratiform, and warm rain) along with sea level pressure (SLP), OLR, and SST. Hereafter, total near-surface rain is referred to as ''total rain.'' Global distributions of total rain, as well as convective and stratiform rains, agree with those found by previous studies based on OLR (e.g., Murakami et al. 1986), which has been used as a proxy of deep convection. Total, as well as compositions of convective and stratiform rains, are strong around tropical monsoon regions, the ITCZ in the tropics, and the subtropical convergence zones (STCZs; Kodama 1992, 1993; Ninomiya 1984, 2007, 2008) in summer; that is, the

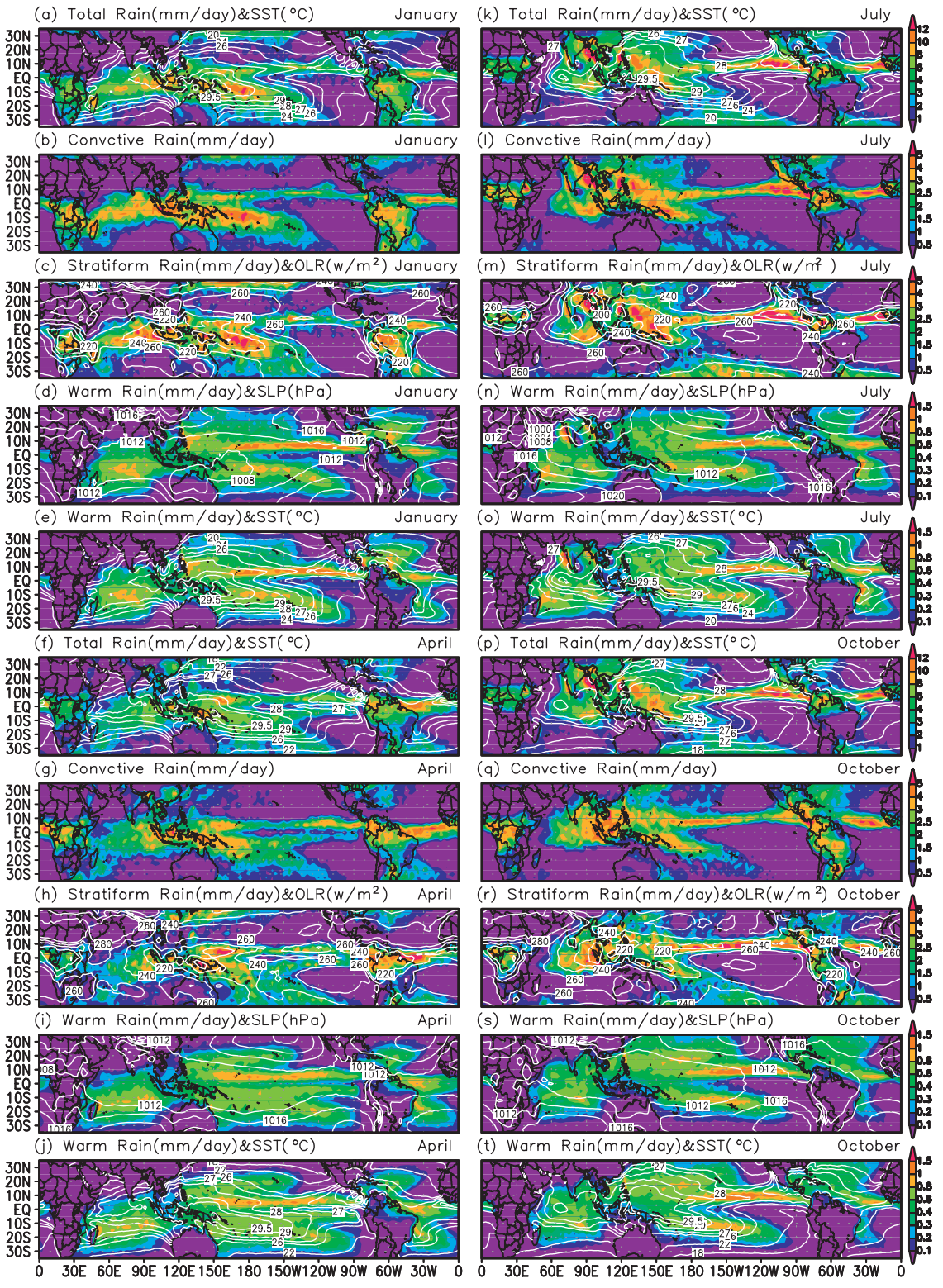

FIG. 1. Near-surface rain categorized by rain type, SST, OLR, and SLP averaged between 1998 and 2006 in January, April, July, and October. Shown are (a),(f),(k),(p) total near-surface rain, (b),(g),(l),(q) convective rain, (c),(h),(m),(r) stratiform rain, and (d),(e),(i),(j),(n),(o),(s),(t) warm rain. SST is shown in (a),(e),(f),(j),(k),(o),(p),(t); OLR in (c),(h),(m),(r); and SLP in (d),(i),(n),(s) by contours.

subtropical portions of the South Pacific convergence zone (SPCZ) and the South Atlantic convergence zone (SACZ) over the Southern Hemisphere (SH) oceans in January and the baiu frontal zone (BFZ) over the western North Pacific in July, and the midlatitude storm tracks in the both hemispheres throughout the year. In these zones, the contribution of convective and stratiform rain is comparable except in the midlatitude storm tracks, where stratiform rain is dominant, but the contribution of convective rain increases in fall and winter. In these seasons, convective rain is ascribed to shallow cells maintained by atmospheric heating from the ocean when cold polar air outbreaks over a relatively warm ocean (Kodama and Tamaoki 2002). Over ocean in the tropics (20°S–20°N), large total rain, as well as the composition of convective and stratiform rains, were observed over regions with higher SST. This is consistent with the dependency of deep convections on SST (e.g., Zhang 1993; Lau et al. 1997). In the subtropics and part of the midlatitudes (20°–35°N and 20°–35°S, hereafter ''subtropics'' despite the inclusion of a part of the midlatitudes), the relationship between SST and rainfall is not straightforward because large rainfall appears along the storm tracks and the STCZs apart from the local SST maximum.

The distribution of warm rain has features unique from those of total, convective, and stratiform rains. Warm rain is confined to areas over oceans, whereas convective and stratiform rains appear over both ocean and land. Short and Nakamura (2000) also showed similar land–ocean contrast for shallow rain. Our results are consistent with the microphysical hypothesis that a low concentration of CCN over oceans favors the development of warm rain through collision–coalescence processes (Beard and Ochs 1984, 1993; Rogers and Yau 1989). The large moisture supply from the ocean to the atmospheric boundary layer is also expected to be favorable for maintaining warm rain.

Except for the North Indian Ocean, the following similar features are found in the distribution of warm rain among oceans (i.e., the North and South Pacific, the North and South Atlantic, and the South Indian Ocean). Warm rain is distributed widely over tropical and subtropical oceans, except over the eastern portions of subtropical oceans. Boundaries of the warm rain coverage in the subtropical oceans seem to be related to SLP fields, and the direction of SLP contours changes near the boundaries. Warm rain extends where contours extend east poleward and disappears where contours extend east equatorward, such as at 90°–120°W and 10°–20°S over the South Pacific (Fig. 1d) and at 130°W and 10°–20°N over the North Pacific (Fig. 1d). Climatically, enhanced subsidence, along with stable air and lowered trade-wind inversion, characterize the eastern portion of the subtropical high (Trewartha and Horn 1980). The subsidence in the eastern part of the high may cause reduced warm rain.

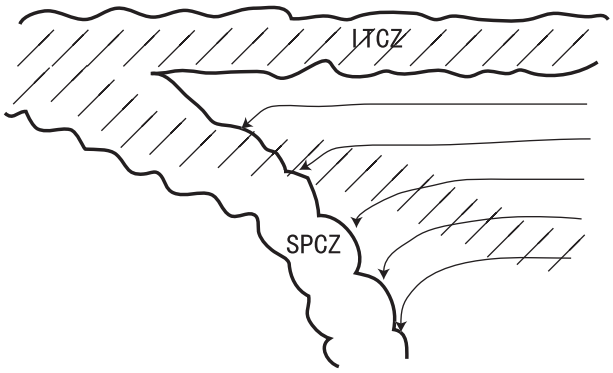

FIG. 2. Schematic view of rainfall over the South Pacific. Thick curves indicate rainbands (ITCZ and SPCZ) of deep convective and stratiform rain. Thin curves with arrows indicate low-level flow toward the SPCZ. Hatch marks indicate the distribution of strong warm rain.

There is a tendency for strong warm rain to appear over oceans with higher SST. In the tropics, total rain and warm rain have similar relationships of rainfall to SST. This is consistent with the findings of Johnson et al. (1999), who reported that congestus clouds coexisted with deep convective clouds in the ITCZ because deep clouds provided snow, which formed a stable layer near the ML by latent heat absorption through the melting of snow (Johnson et al. 1996). In the subtropics, the dependence on SST is more significant for warm rain than for total rain. As a result, warm rain and total (or convective and stratiform) rain show different distributions around the STCZs and the midlatitude storm tracks. For the SPCZ and SACZ in summer (Figs. 1a and 1e), the zone of maximum rainfall in total rain appears over the local SST maximum in the tropics but extends southeastward across the contours of SST in the subtropics. In contrast, strong warm rain is distributed more zonally along the local SST maximum. Warm rain is also weak in the BFZ in early summer at 30°–35°N and 120°–150°E (Figs. 1k and 1o), which is a significant STCZ having large total rain values. The STCZs are supplied with moisture by low-level flow along the western periphery of the subtropical high (e.g., Shinoda et al. 2005). In the upstream of low-level northeasterly flow for the SPCZ and SACZ, and in the southwesterly flow for the BFZ, SST is higher and warm rain is fairly strong. The contrasting features between the ITCZ and STCZs for warm rain are a novel finding of this study. Figure 2 shows these situations schematically. In the midlatitude storm tracks with large total rain at ~35°N and ~35°S over oceans, warm rain is weak with a seasonal increase

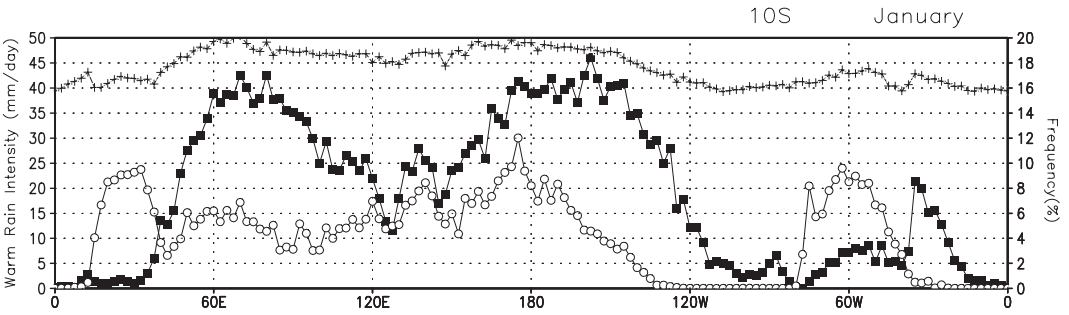

FIG. 3. Warm rain intensity averaged for pixels where warm rain was detected (line marked with closed boxes, scaled on the left ordinate), frequency of warm rain (line marked with crosses, scaled on the right ordinate), and frequency of precipitation at 6 km MSL (line marked with open circles, scaled on the right ordinate) along 10°S in January averaged between 1998 and 2006.

in fall and winter. This result is ascribed to shallow cells developed in unstable air when cold air outbreaks over relatively warm oceans after the passage of cyclones because shallow convection increases along storm tracks in these seasons (Kodama and Tamaoki 2002).

The distribution of warm rain is also related to topography. Strong warm rain is found on the upwind side of coasts with mountain ranges. Examples include the east coasts of the Philippines and equatorial Central America in January when trade winds are strong (Fig. 1d), and the west coasts of India and the Indochina Peninsula in July when the southwest monsoon prevails (Fig. 1n). Xie et al. (2006) noted that mesoscale mountain ranges in the Asian monsoon region maintain strong rain on their windward sides and used numerical experiments to show that LH by such terrestrially induced rainfall intensifies monsoon circulation. However, they did not discuss the vertical structure of the rainfall. We found a large contribution of warm rain in terrestrially induced rain.

The rainfall distribution over the North Indian Ocean is unique. There, to the south of 10°–15°N, fairly strong warm rain extends over the whole ocean; in contrast, warm rain is scarce over the eastern portions of the other oceans. Warm rain is scarce to the north of 10°–15°N throughout the year, except along the west coast of India and the Indochina peninsula in summer, where an upwind portion of the monsoon westerly occurs. The subtropical high is weak over the North Indian Ocean throughout the year. This may cause unique characteristics of rain distribution and requires further study.

Over land in the tropics and the subtropics, warm rain increases in summer over part of the Indochina peninsula in July and October (Figs. 1o and 1t) and over the northern part of South America in January and April (Figs. 1e and 1j), although the contribution to total rain is ~2%, as shown later. These seasons are the middle and late wet seasons when the boundary layer over tropical rain forests is expected to be very humid. Warm rain is weak throughout the year over the Congo rain forest of equatorial Africa. Continental features of rainfall over the Congo are remarkable even in wet seasons (Petersen and Rutledge 2001).

Seeking an explanation for the significant land–ocean contrast of warm rain intensity, we examined the frequency of warm rain and warm rain intensity averaged for pixels in which warm rain was detected. Figure 3 shows 9-yr averages of these amounts along 10°S in January as an example. The frequency of warm rain occurrence normalized by the frequency of PR observations is almost even over both ocean and land areas (16%–20%). However, there were large differences in the intensity of warm rain averaged for cases of detected warm rain occurrence: the large amount of warm rain shown around 60°–90°E and 180°–160°W (areas of relatively strong warm rain, as illustrated in Fig. 1e) contrasts with the near-zero amount of warm rain over the continents and eastern parts of the oceans (20°W–30°E and 110°–40°W). The amount of warm rain depends on the warm rain intensity for warm rain events, not on the frequency of the occurrence of warm rain, which is relatively flat. Figure 3 also shows the frequency of precipitation echoes at 6 km MSL above the ML to examine disturbances in warm rain observations by upper-level echoes. The echo frequency increases around 160°E–160°W and 40°–80°W. However, there is no significant decrease in warm rain frequency according to the increased frequency of upper-level echoes. This suggests that upper echoes have no influence, or a nondominant influence, on warm rain observation.

Figure 4 shows the low-level cloudiness distribution derived from ISCCP-D2 data in the four months examined. In the ISCCP-D2 data, low-level cloudiness is defined as the area coverage ratio of clouds with tops below the 680-hPa level. Low-level clouds covered by middle- or upper-level clouds are not included in low-level cloudiness. The statistics of low-level cloudiness

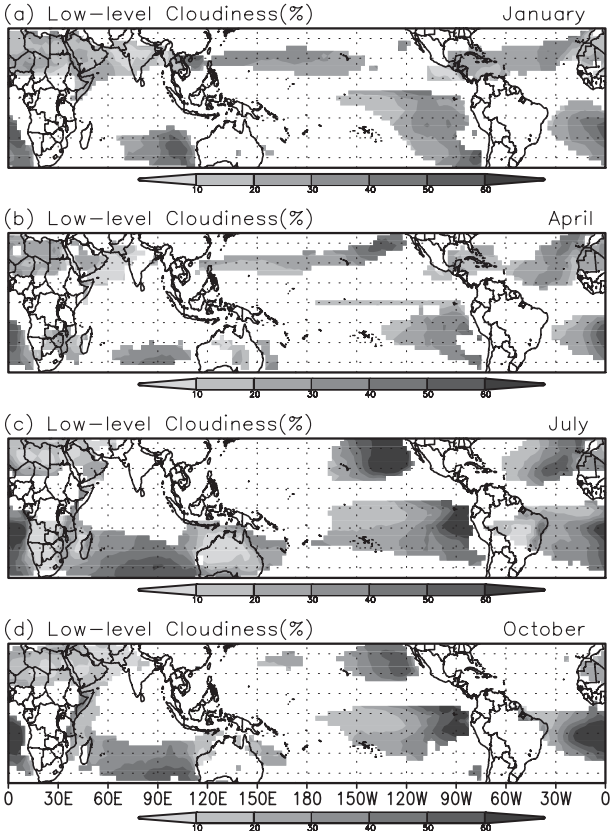

FIG. 4. Low-level cloudiness in January, April, July, and October derived from ISCCP-D2 data averaged between 1998 and 2006. Low-level cloudiness is not shown where the summation of mid- and upper-level cloudiness was more than 30% because large cloudiness in these categories disturbs satellite observation of low-level cloud.

are thus not reliable where mid- or upper-level cloudiness values are large. Climatic air temperature at the 680-hPa level is approximately 10°C over the tropical oceans, but it varies between −10° and 20°C in the midlatitudes. Therefore, except in the midlatitudes in winter, the rainfall from low-level clouds should be warm rain, although a part of the warm rain was from midlevel clouds defined as having tops between 680 and 440 hPa. Figure 4 shows the distribution of low-level cloudiness where the summation of upper- and midlevel cloudiness is less than 30%, although the influence of upper and middle clouds on low-level cloudiness may remain despite this treatment. Warm rain is weak where low-level cloudiness is substantial. For example, over the eastern portion of the subtropical oceans, except for the North Indian Ocean, low-level cloudiness is extensive (more than 40%), where subsidence is strong and warm rain, as well as total rain, is weak.

To demonstrate how rainfall depends on SST and cloudiness, several scattergrams were prepared. Figure 5 shows the relationship between monthly averaged total and warm rain to SST in January, which is winter (summer) in the Northern Hemisphere (NH; SH), for the nine years. In the tropics (20°S–0° and 0°–20°N), total rain rapidly increases when SST exceeds 27°C (Fig. 5b). This result seems to coincide with the findings of Zhang (1993) and Lau et al. (1997), who pointed out that OLR decreased above 27°C. In the subtropics and a part of the midlatitudes in winter, the relationship between SST and rainfall is weak or reversed (Fig. 5a); this result reflects the high total rain in winter along midlatitude storm tracks where SST is relatively low in the study area. However, warm rain shows a clear positive correlation to SST (Fig. 5d), although the critical SST above which warm rain increases is higher in the tropics than in the subtropics (cf. Fig. 5d versus 5e). This result is consistent with Johnson et al.'s (1999) report of positive correlation between the number of congestus and SST in the TOGA COARE area. The critical SST above which rainfall increases is somewhat lower for warm rain (~24°C) than for total rain (27°–28°C) in the tropics (cf. Fig. 5d versus 5e). This finding is consistent with that of Masunaga et al. (2005), who noted that shallow rain appeared at SSTs lower than the critical SST for an increase of total rain in the tropical Pacific.

Figure 6 shows the relationship between the monthly averaged precipitation and cloudiness in January for the nine study years. Low-level cloudiness is plotted only when the summation of upper- and middle-level cloudiness is less than 30%, although an influence of upper and middle clouds on the statistics of low-level cloudiness may remain despite this treatment. Total rain is well correlated with upper-level cloudiness in the tropics and subtropics in summer (Figs. 6b and 6c), indicating that most rain is provided by deep stratiform and convective clouds extending to the upper troposphere. In the tropics and subtropics in summer, the relationship between warm rain and low-level cloudiness is scattered; however, negative correlation is found between them (Figs. 6e and 6f). Warm rain nearly disappears when low-level cloudiness exceeds 40%, but it reaches maximum values when low-level cloudiness is around 20%–30%. More convective clouds are expected when cloudiness is 20%–30% than when cloudiness exceeds 40%. The latter may correspond to stratocumulus or stratus, although quantitative correspondence between cloudiness and cloud type has not been examined. This finding indicates that shallow convective clouds provide warm rain and is consistent with the suggestion that strong warm rain is provided by shallow clouds with updraft (Houze 1993, chapter 6). In winter in the subtropics, the relationships between upper cloudiness and total rain and between low-level cloudiness and warm rain are unclear and very scattered

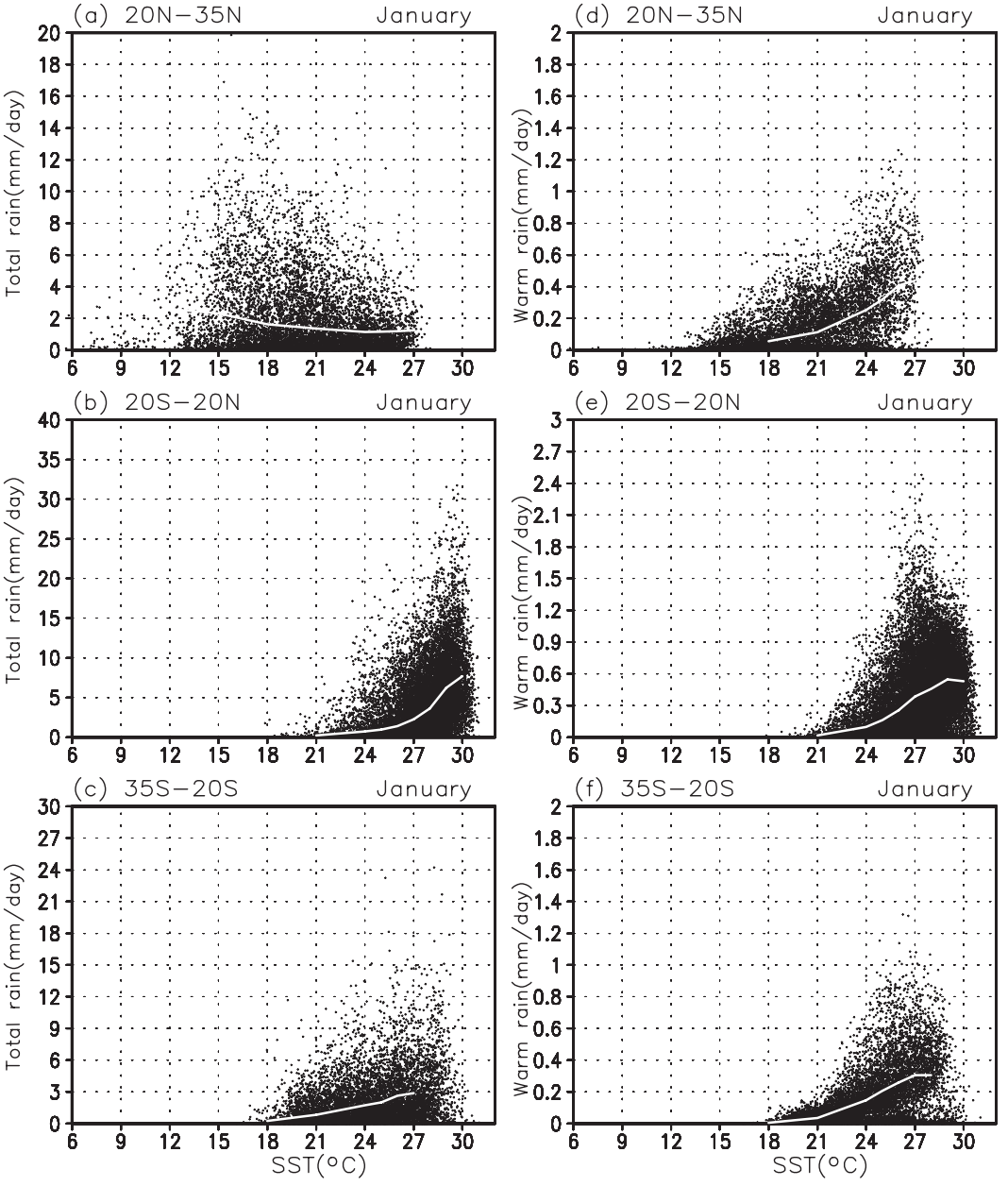

FIG. 5. (left) Scattergrams between monthly averaged total near-surface rain and SST over three latitude zones in January averaged between 1998 and 2006. (right) Same as in (left) but for warm rain and SST. White curves indicate mean rainfall for each SST.

(Figs. 6a and 6d). In these seasons, midlatitude storm tracks shift to lower latitudes into the study areas and modify the relationship. We found similar relationships in other months as well (April, July, and October), although relationships in the subtropics in spring and fall are similar to those in the subtropics in summer (not shown).

Figure 7 shows the seasonal variation of near-surface rain of each type over 12 reference regions, categorized by land/sea conditions and latitudes of the tropics and the subtopics in each hemisphere. Flash rates and ratios of warm and convective rains to total rain are also shown. A high flash rate is expected in convective clouds with much graupel (e.g., Cecil et al. 2005; Kodama et al. 2007). The seasonal variations of convective and stratiform rains, flash rates, and their land–sea contrast are consistent with those reported by previous studies (e.g., Kodama et al. 2005). The ratio of warm rain is low (2%–5%) throughout the year over land and varies

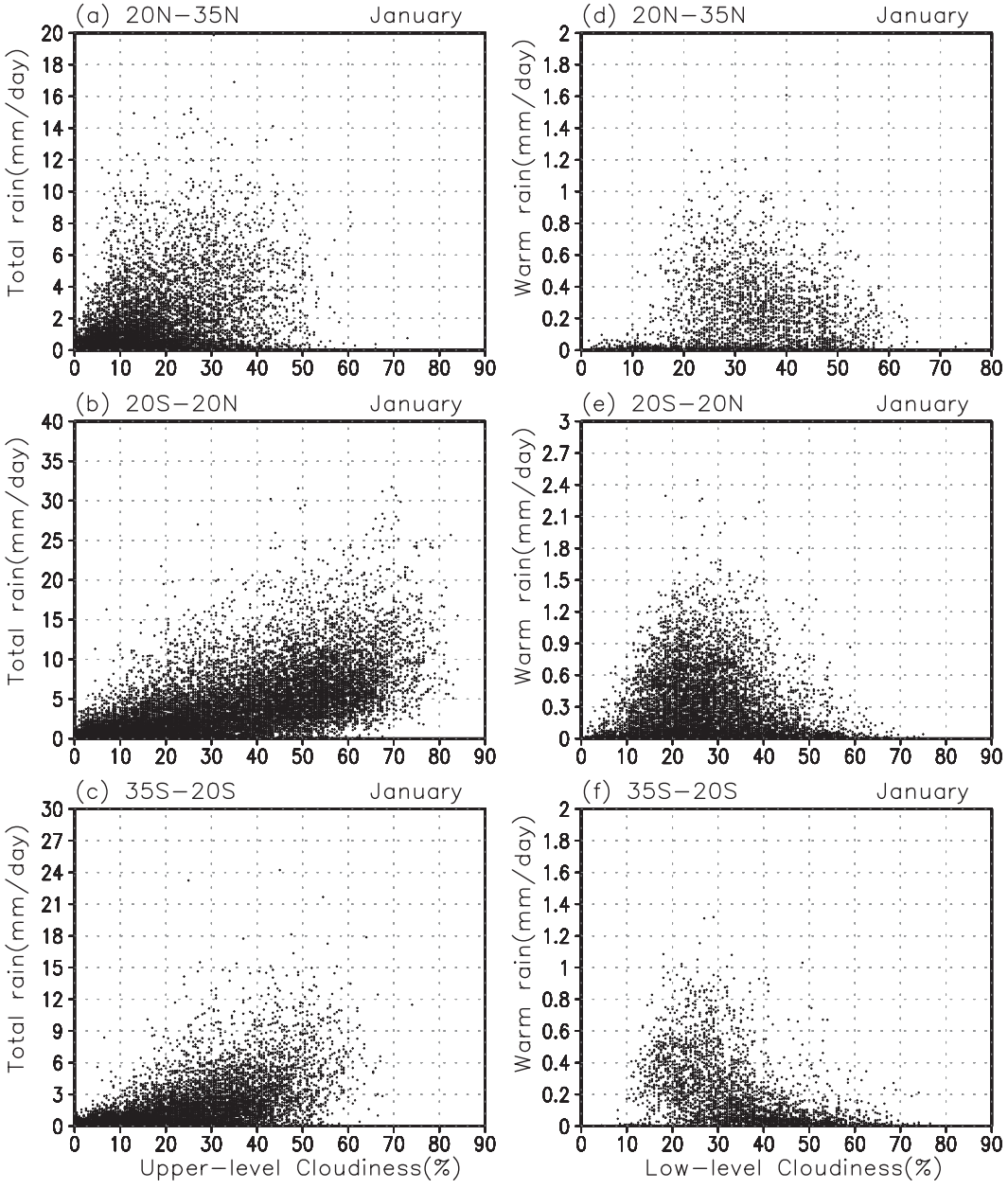

FIG. 6. (left) Scattergrams between monthly averaged total near-surface rain and upper-level cloudiness over three latitude zones in January averaged between 1998 and 2006. (right) Same as in (left) but for warm rain and low-level cloudiness for the areas where the summation of mid- and upper-level cloudiness was less than 30%.

between 10% and 20% over the ocean. The ratio of warm rain over oceans increases in winter when total rain is minimal in the tropics and in summer and fall in the subtropics. Seasonal variation of the warm rain ratio in the tropical oceans is related to the seasonal migration of the ITCZ. In winter, the ITCZ with strong convective and stratiform rain shifts to the summer hemisphere, and the contribution of warm rain increases in the winter hemisphere covered by subtropical highs. Over the subtropical oceans, the increase in warm rain in summer and part of fall is ascribed to the seasonal poleward extension of subtropical highs, which develop warm rain in the western portion. The fall increase is also ascribed to shallow convections developing in unstable air when cold air outbreaks over the relatively warm ocean after the passage of cyclones. Such precipitation is likely to be classified as warm rain in fall but as convective rain in winter because of low air temperatures.

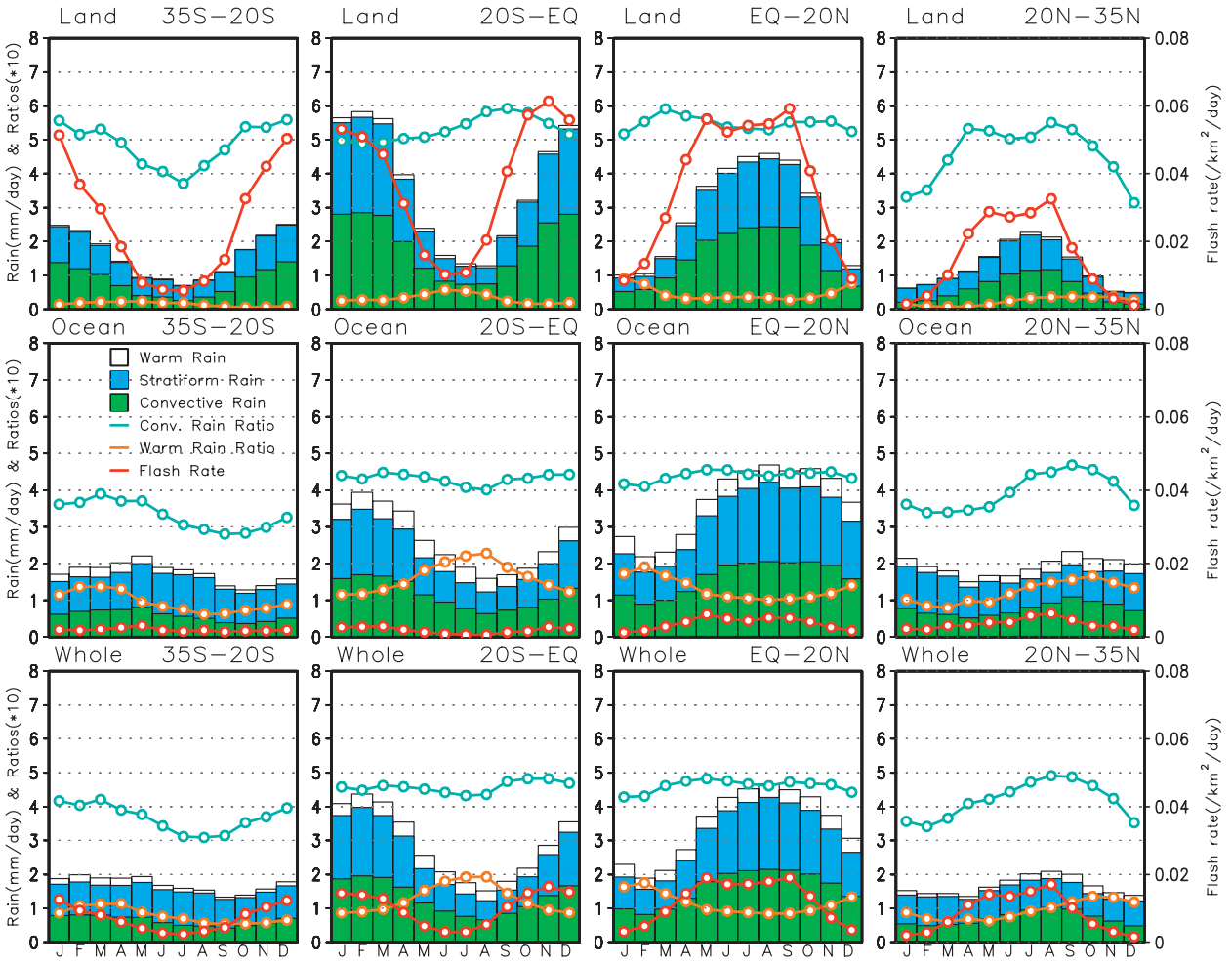

FIG. 7. Seasonal variation of near-surface rain (bar graph scaled on the left ordinate), flash rate (red line graph scaled on the right ordinate), and ratios of warm rain and convective rain (orange and blue line graphs, respectively, scaled on the left ordinate) averaged for 12 regions classified by latitude and land/sea conditions. The near-surface rain is classified into convective (green bar), stratiform rain (blue bar), and warm rain (white bar) for (top) land, (middle) ocean, and (bottom) entire area, including land and ocean.

5. Latent heating

To illustrate the vertical structure of LH profiles, Fig. 8 shows annual-mean LH profiles and the composition of each rain type averaged for the 12 reference regions adopted in Fig. 7. A positive peak in total LH profiles is found at 5–6 km MSL, although the peak height is somewhat greater in the tropics over both land and ocean areas. Both stratiform and convective rains contribute to the formation of the positive peak in the midtroposphere. Stratiform rain forms positive LH values in the midtroposphere, peaking at 6–7 km MSL in the tropics (~6 km MSL in the subtropics), and negative LH values in the lower troposphere at 3–4 km MSL in the tropics (~2 km MSL in the subtropics). Convective rain shows a single-mode positive LH peak at 4–5 km MSL in the tropics (~3–4 km MSL in the subtropics), although the positive peak is higher over land. Negative LH values for convective rain form in the lower troposphere over land. These features in LH profiles over ocean in the tropics are consistent with simulations of several maritime areas by a cloud-resolving model (Shige et al. 2007), although the positive LH peak in our results is 1–2 km lower. We will examine these LH profiles in comparison to the findings of previous studies of heat and moisture budget analyses in section 6. In the lower troposphere (1–3 km MSL), total LH is negative over land as a result of cooling by stratiform rain and partially convective rain. However, total LH is positive over the oceans as a result of heating by warm rain distributed over ocean areas.

Figure 9 shows the LH distribution at 1.5 km MSL in January and July. Total LH and the composition of LH for convective, stratiform, and warm rain are shown. In

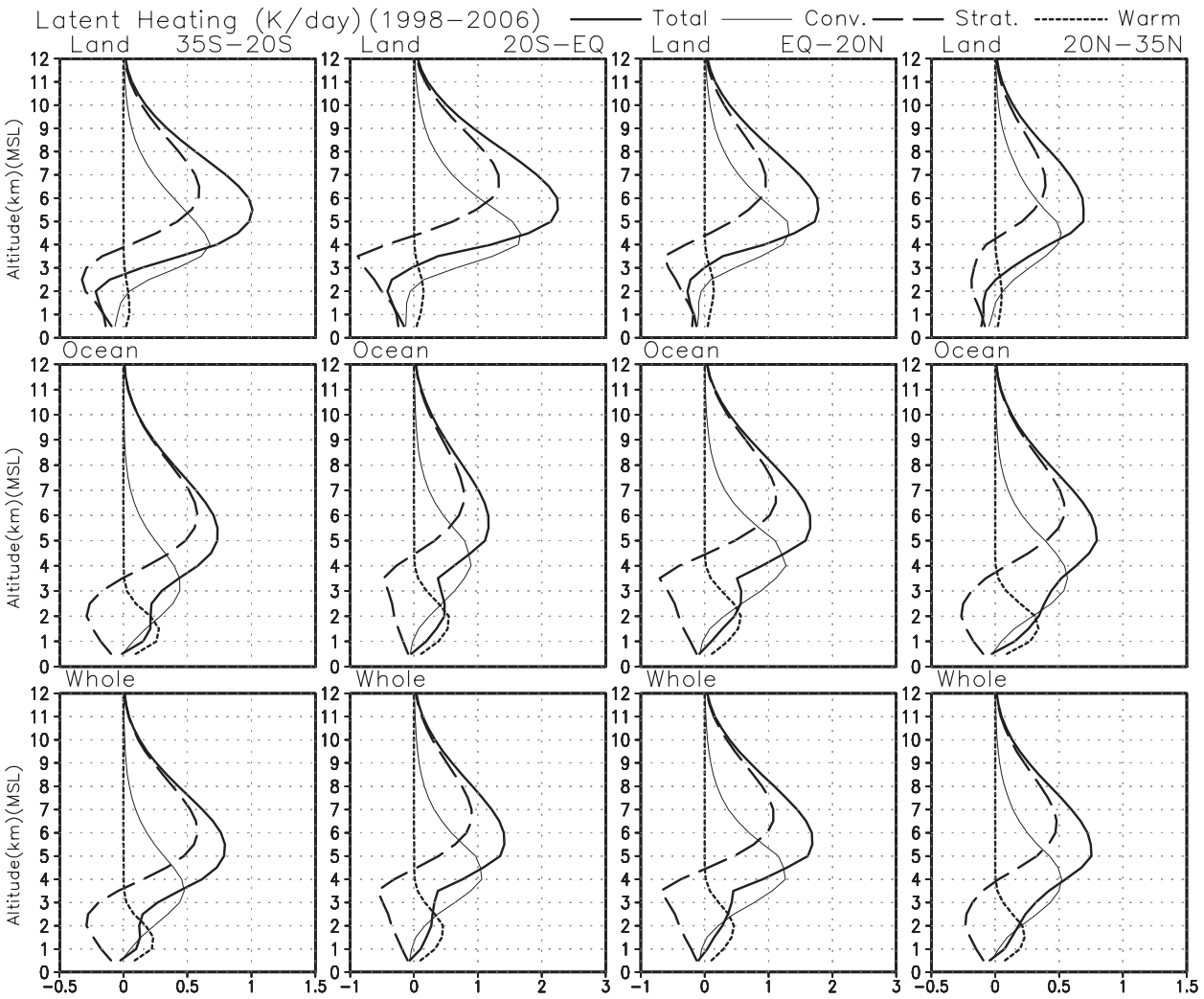

FIG. 8. Profiles of annual mean LH averaged for the 12 regions in Fig. 7. Thick solid lines indicate the LH profiles, thin solid lines indicate LH by convective rain, long-dashed lines indicate LH by stratiform rain, and dotted lines indicate LH by warm rain.

the tropics, strong cooling is observed over continents, especially in the summer hemisphere. Positive heating is widely distributed over the ocean, especially along the ITCZ and the subtropical portions of oceans (i.e., the South Indian Ocean and western parts of the subtropical North Pacific and North Atlantic). Warming is also strong along the warm rain maximum to the northeastern side of the STCZs in the SH (cf. Figs. 1d and 1n). Along the STCZs in summer, cooling or weak warming is evident. This is a result of weak warm rain, which cannot compensate strong cooling by stratiform rain along these zones. In winter, strong positive LH appears along storm tracks in the midlatitudes, especially in the NH and along the southeast coast of Australia. This strong heating is maintained by convective and warm rains and will be examined in detail later. Because positive LH is concentrated over oceans, the LH contrast between the ocean and land is substantial along the coast, reaching 1–2 K day^{-1} around the northeast and southeast coasts of South America in January. The large LH contrast across coasts may affect local and monsoon circulations.

Figure 10 shows the LH distribution at 10 and 6 km MSL, the composition of each rain type at 6 km MSL, and the OLR. At 10 km MSL, positive LH is observed over the continents as well as the warm water pool over the Indian Ocean and the western Pacific. LH values are fairly large along the ITCZ. This distribution agrees with those of lower OLR. At 6 km MSL, where a positive peak likely appears in LH profiles (cf. Figure 8), positive LH is found over regions similar to those at 10 km MSL. Moreover, large positive LH extends to the STCZs, subtropical continents, and midlatitude storm tracks in warm seasons. These extensions of large LH values are

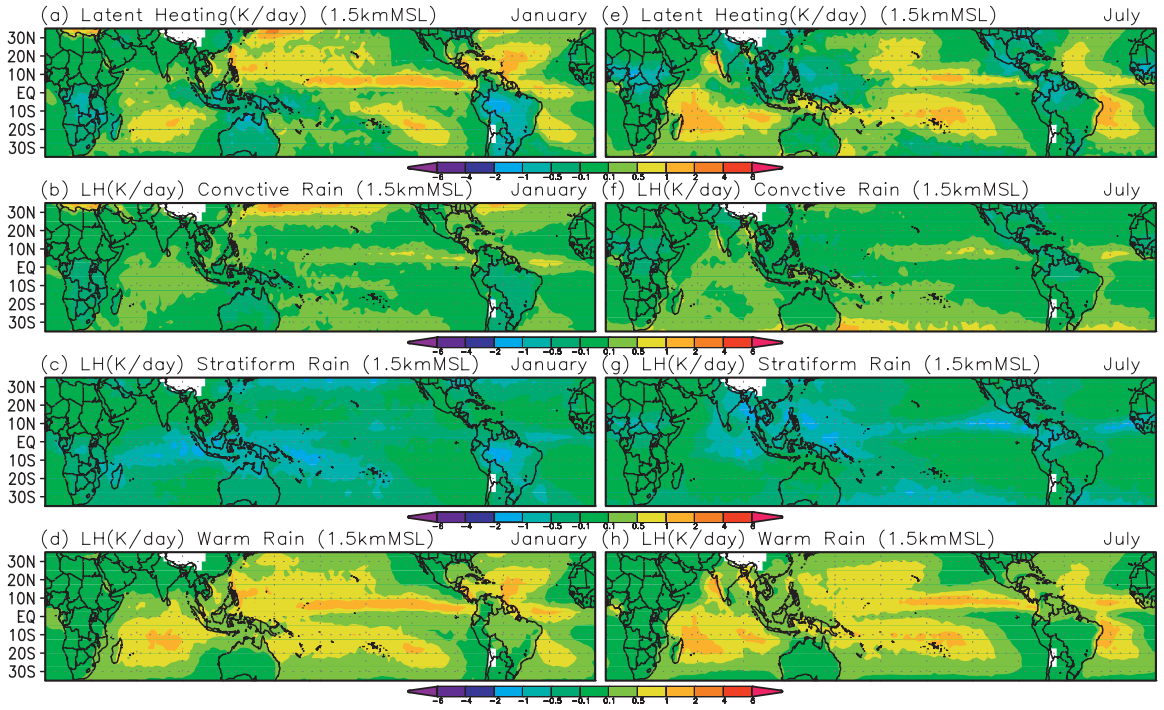

FIG. 9. Distribution of LH at 1.5 km MSL in January and July averaged between 1998 and 2006. (a),(e) LH by total rain, (b),(f) LH compositions of convective rain, (c),(g) stratiform rain, and (d),(h) warm rain are also shown.

explained by stratiform rain over oceans and both convective and stratiform rains over continents. OLR is a proxy of these positive LH values at 6 km MSL, although large positive LH over the subtropical and midlatitude oceans is weakly represented in OLR fields because the top height of rain is somewhat lower despite the strong rain over these areas. The OLR does not represent the positive LH distribution in the lower troposphere (cf. Fig. 9). In the tropical oceans, low OLR is related to negative or nearly zero LH values, such as those over the tropical western Pacific where deep stratiform rain causes low-level cooling.

Figure 11 shows the seasonal variation in LH profiles for the 12 reference regions adopted in Fig. 7. Over land, cooling in the lower troposphere and warming in the midtroposphere are significant. Low-level cooling and midtropospheric heating are intensified in summer. In the subtropics, the height of the boundary between cooling and warming changes seasonally because of seasonal migration of the ML height. Over oceans, cooling in the lower troposphere is scarce because LH by warm rain over the oceans compensates cooling by stratiform rain. In the subtropics, low-level heating is intensified in fall and winter, when shallow convective rain, along with warm rain, is intensified over oceans where the air–sea temperature difference is greater. In the tropics, the LH contrast between cooling over land and warming over oceans is maintained throughout the year and is accompanied by seasonal variation.

Figure 12 shows the seasonal variation of LH categorized by rain type at 1.5 km MSL for the 12 reference regions adopted in Fig. 7. Over land, negative LH by stratiform rain is intensified in the warm season in both the tropics and subtropics. This cooling is not compensated by the heating of rain in other categories. Negative LH by stratiform rain shows similar seasonal change between the ocean and land. Over the ocean, strong heating by warm rain is found in the tropics. Note that the contribution of warm rain to LH in the lower troposphere is predominantly large despite the small contribution of warm rain to total rain in rainfall amount. In the subtropics, positive LH by convective and warm rain is also intensified in fall and winter, corresponding to shallow convections that develop in these seasons when the air–sea temperature difference is large. As a result, total LH is positive throughout year in the tropics and the subtropics over most oceans.

Seasonal variation of LH at 6 km MSL is shown for the 12 reference regions (Fig. 13). At this altitude, LH is positive over both land and oceans. The LH is ascribed to convective and stratiform rains, and the contribution of warm rain is negligible. Over land, LH increases in summer. Over ocean, the seasonal phase change of LH is delayed by 1–2 months from that over land. The

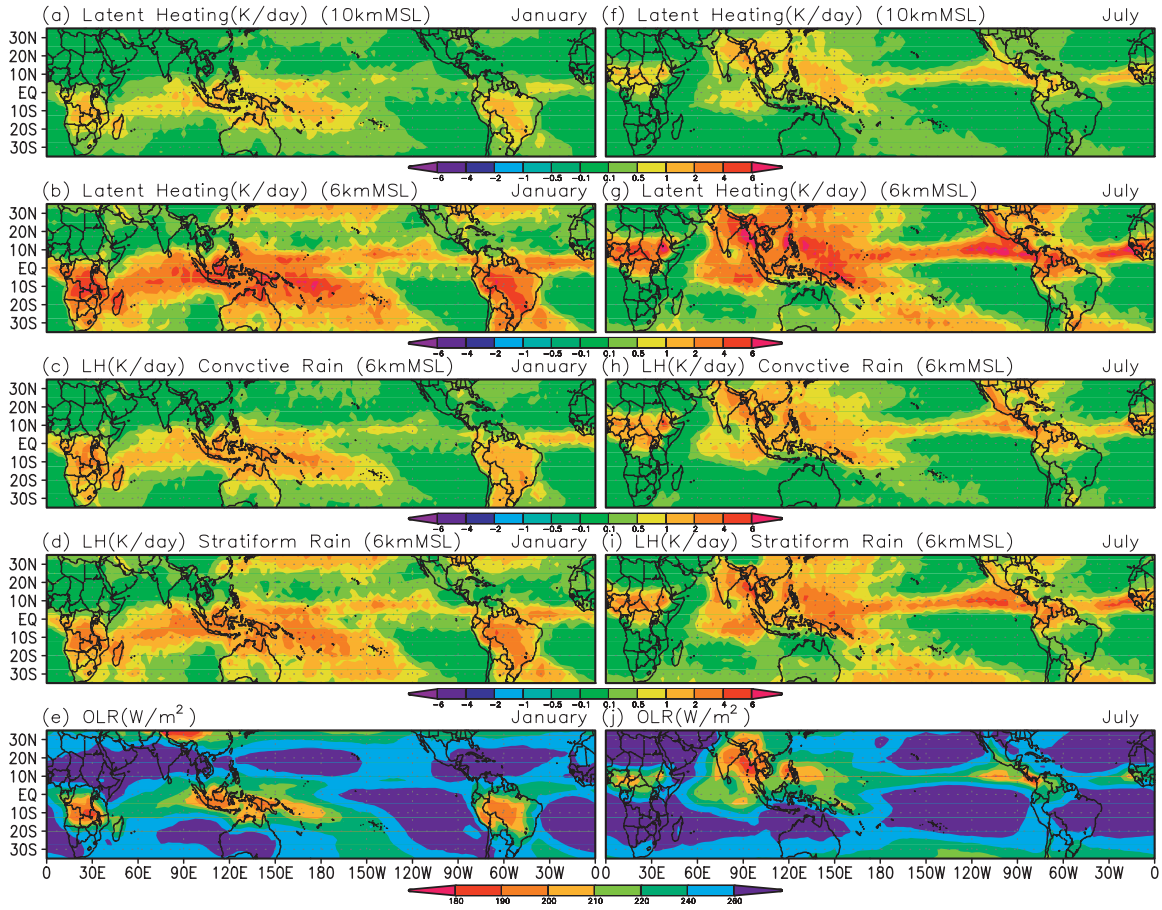

FIG. 10. Same as Fig. 9 but for (a),(f) total LH at 10 km MSL and (b),(g) 6 km MSL. Composition of (c),(h) LH at 6 km MSL is shown for convective rain and (d),(i) stratiform rain. (e),(j) OLR is shown.

contribution of convective rain is larger in the tropics than in the subtropics.

6. Characteristics in specific regions and comparison to previous studies

Warm rain intensity and accompanying LH evaluated by the PRH algorithms are difficult to confirm by ground-based observations. With this issue in mind, in this section we compare our results for several specific areas to those of previous studies of rainfall observation and heat and moisture budget analysis. Figure 14 marks the locations of the reference areas with varying geographic conditions. Some of the areas were selected from the fields of the following previous campaigns: EPIC in eastern equatorial Pacific (Raymond et al. 2004; j), TRMM Large-scale Biosphere–Atmosphere Experiment in Amazonia (TRMM-LBA, Silva Dias et al. 2002; k), TOGA COARE in the western Pacific (Webster and Lukas 1992; h) and the Mirai Indian Ocean cruise for the Study of the MJO-convection Onset (MISMO, Yoneyama et al. 2008; i). Figure 15 is the same as Fig. 7 except for the reference areas. The ratio of warm rain is large over oceans, especially for the ITCZ and the warm water pool, throughout the year (10%–20%) in the tropics (e.g., Figs. 15g–15j) and in the western portion of subtropical highs (10%–40%) in the subtropics (e.g., Fig. 15f). The ratio also increases in summer over the west coast of India, where the onshore summer monsoon prevails (10%–20%; Fig. 15c). In the midlatitudes, warm rain increases in summer and fall over storm tracks (5%–10%; e.g., Figs. 15b and 15l). Short and Nakamura (2000) showed that the contribution of shallow rain with tops of ~2 km MSL accounts for around 20% of the total rain over the tropical and subtropical oceans. They also noted that the contribution decreased in the ITCZ to ~5%. Our results for warm rain are somewhat larger for the ITCZ (10%–20%) and subtropical oceans (10%–40%). The positive bias is reasonable considering the contribution of cumulus congestus (Johnson et al. 1999), which was not included in the shallow rain defined by Short and Nakamura (2000).

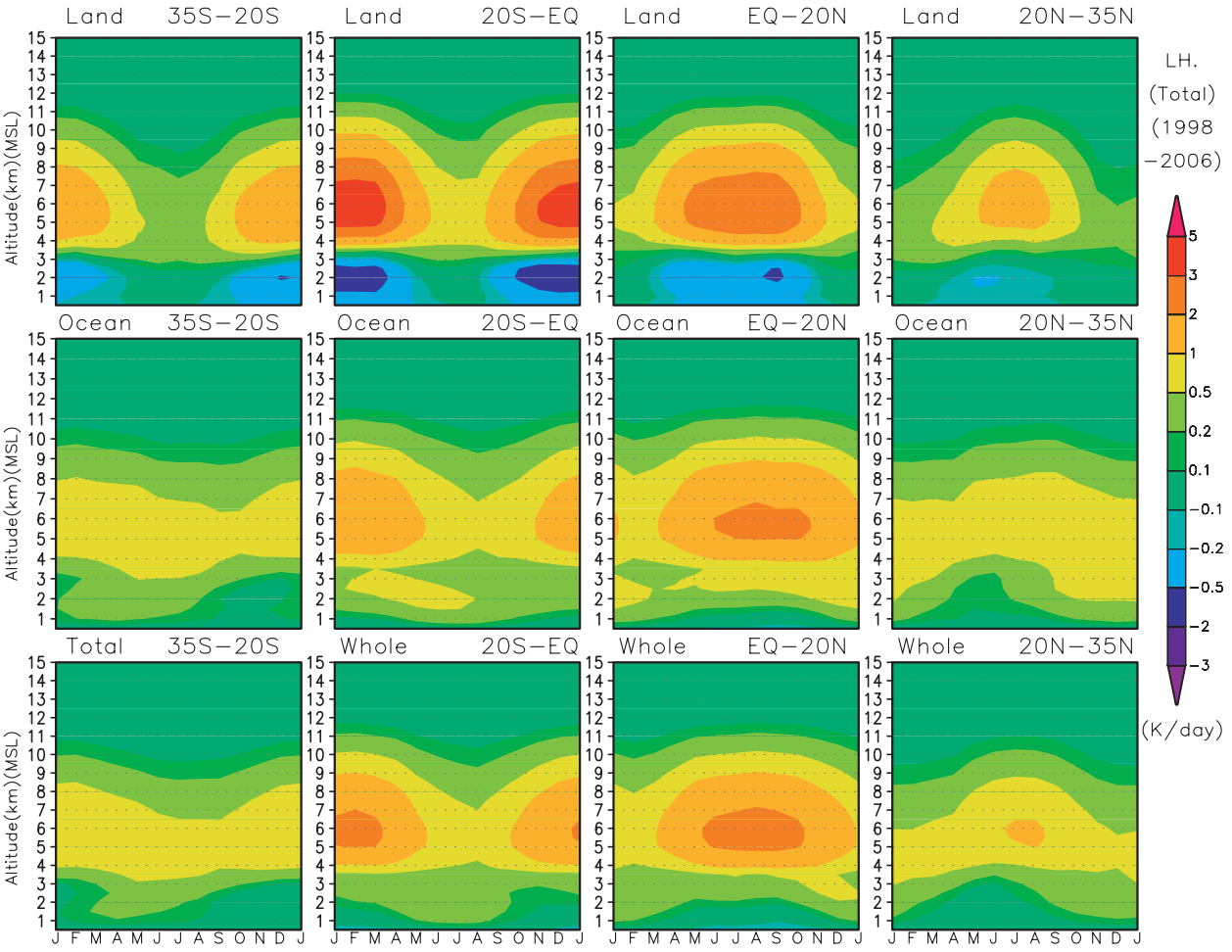

FIG. 11. Seasonal variation of LH profiles averaged for the 12 regions in Fig. 7.

Warm rain is observed over tropical rain forests in wet seasons, although with small contributions (~2% or less; e.g., Fig. 15k). Pereira and Rutledge (2006) showed that shallow convection contributed to approximately 10% of the total rainfall obtained from ground radar observations in the TRMM-LBA area during the wet season in the Amazon. In our results, the contribution of warm rain is ~2%. Pereira and Rutledge (2006) also found that warm rain was stronger in the wet season (January and February 1999) over the Amazon (TRMM-LBA) than in the ITCZ over the eastern Pacific in fall (September and early October 2001) over the EPIC area. This contradicts our results, indicating stronger warm rain in the ITCZ over the eastern Pacific (cf. Fig. 15j versus Fig. 15k). The horizontal resolution of TRMM PR (4.3 or 5.0 km) may not be enough to describe small-sized rainfall systems, which may dominate over land (Short and Nakamura 2000). This may cause an underestimation of warm rain over land. Other causes of the difference may be differing definitions of warm rain and the performance of observation instruments; for example, the lower limit of radar signals for TRMM PR (~18 dBZ) may be higher than those for ground-based radars. Few observational studies of warm rain by ground-based radar have been conducted, but they are expected to confirm the results for warm rain derived from TRMM observations.

Next, we examine Q1 and Q2 profiles in the lower troposphere described in previous studies and compare them to our LH profiles. Using TOGA COARE data, Lin and Johnson (1996) showed a lower tropospheric positive Q1 (apparent heat source) and positive Q2 (apparent moisture sink) peaking at the 850-hPa level around the ITCZ at around 5°N and 5°S, and the disappearance of the low-level peak near the equator over the western Pacific (their Fig. 13). Because the coexistence of an apparent moisture sink and an apparent heat source suggest latent heating by the condensation process, their results are consistent with our large low-level positive LH at ~2 km MSL along the ITCZ, maintained by warm rain (Figs. 16g, 16i and 16j) and negative LH

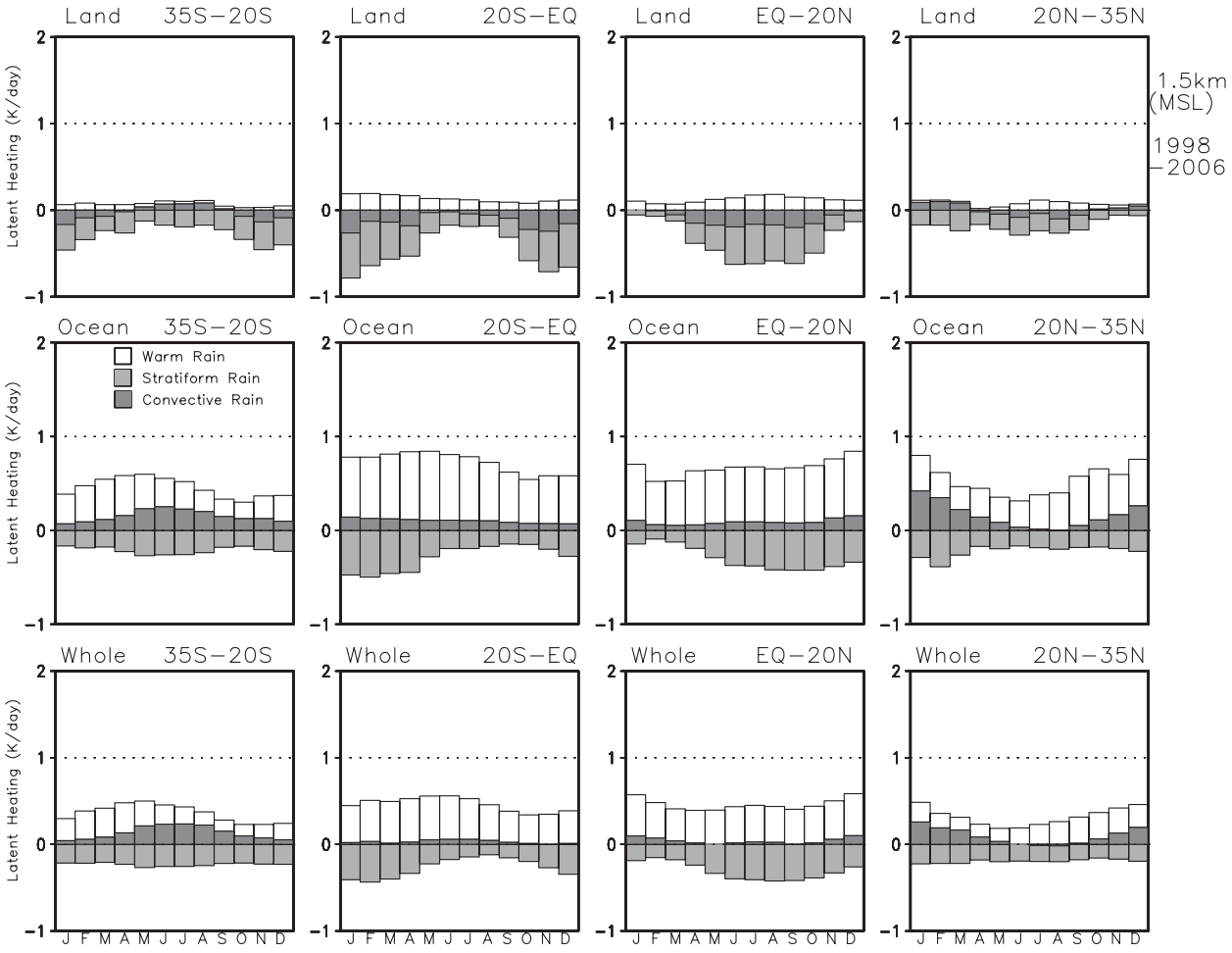

FIG. 12. Seasonal variation of LH at 1.5 km MSL categorized by rain type for the 12 regions in Fig. 7.

near the equator (Fig. 16h). Luo and Yanai (1984) examined Q1 and Q2 around Bangladesh and the Bay of Bengal, and over the South China plain around the Yangzi River basin, using level II-b data from the first Global Atmospheric Research Program (GARP) Global Experiment for early summer. In the lower troposphere, large positive LH was suggested by larger positive Q1 and Q2 over the Bangladesh and Bay of Bengal area, whereas weaker positive LH was suggested by small Q1 and Q2 over the South China plain. Our results also show contrasting LH between these areas in early summer (June), with nearly zero LH at 1.5 km MSL (Figs. 16d and 16e) over Bangladesh and the northern part of the Bay of Bengal and negative LH at 1.5 km MSL (Fig. 16a) over South China. Schumacher et al. (2007) pointed out that the low-level peak of Q1 profiles around the 750-hPa level, which suggests a low-level positive LH peak, was found in the ITCZ over the central Pacific (Kwajalein field experiment) but not in the South China Sea and Amazon (TRMM-LBA field). Over the Amazon, strong negative Q1 in the lower troposphere was found around midnight where stratiform rain was dominant. These results are consistent with the difference in low-level LH profiles among regions in our study; we found a positive LH in the ITCZ in the lower troposphere almost throughout the year (Figs. 16g, 16i, 16j) and negative LH over the Amazon (Fig. 16k). Yanai and Tomita (1998) examined the seasonal variation of Q1 and Q2 profiles over Bangladesh and the northern part of the Bay of Bengal. Large Q1 and Q2 in the lower troposphere, indicating positive LH, were shown only in summer. This finding is consistent with our results, in which low-level cooling is weakened in midsummer (Figs. 16d and 16e). The correspondence is not perfect. Strong low-level negative LH is found over Amazon in SH summer (Fig. 16k), whereas daily mean Q1 is not negative (Schumacher et al. 2007; Yanai and Tomita 1998). Large seasonal changes of LH in the lower troposphere below 2 km MSL over the western Pacific off the Philippines—that is, positive in winter and negative in summer (Fig. 16f)—are not

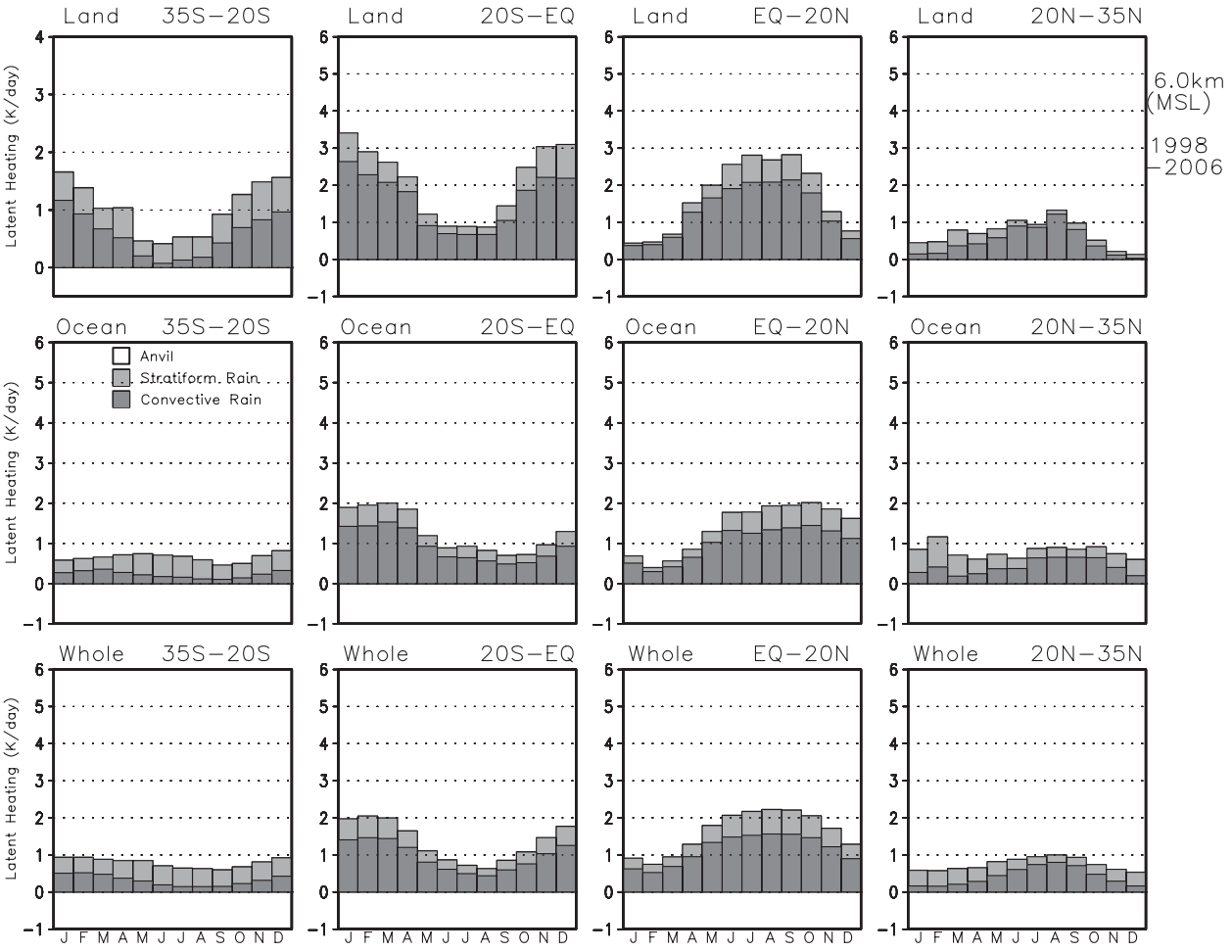

FIG. 13. Same as Fig. 12 but for 6 km MSL.

consistent with the corresponding analysis of Q1 and Q2 by Yanai and Tomita (1998). The PRH algorithm may overestimate lower-tropospheric cooling as a result of an underestimation of the warming by warm rain over these areas. A possible reason for these disagreements is examined in section 7.

Continuing with the examination of the LH profiles given in Fig. 16, low-level positive LH is maintained throughout year in the ITCZ over the eastern Pacific (Fig. 16j), whereas negative LH appears with strong cooling by stratiform rain in the ITCZ in the western North Pacific and Indian Ocean in summer and fall (Figs. 16g and 16h). Over the Asian summer monsoon regions (Figs. 16c–16e), low-level cooling along with deep, strong positive heating in the midtroposphere appears (approximately in May) before the onset of the southwest monsoon. However, low-level cooling is then weakened after the onset of the monsoon due to the increase of LH by warm rain. This result is consistent with reports that latent heating in the premonsoon period serves as a conditioning process during the onset of Asian summer monsoon (Ueda et al. 2003; Kiguchi and Matsumoto 2005). Along storm tracks over the North Pacific, strong low-level cooling appears in early summer (Fig. 16b), when the storm track is in the BFZ. Strong cooling in the lower troposphere in the BFZ is ascribed to strong cooling by stratiform rain and weak warming by rare warm rain (not shown). In low-level cooling, LH is weakly positive or weakly negative for the SPCZ (Fig. 16i) and SACZ (not shown) in summer of the SH.

7. Summary and future tasks

We studied the large-scale distribution of precipitation and LH profiles using a 9-yr dataset derived from TRMM PR observations, with emphasis on the contribution of warm rain. The distribution of warm rain shows unique features that contrast with those of rain in other categories and of OLR. Warm rain is intense over oceans.

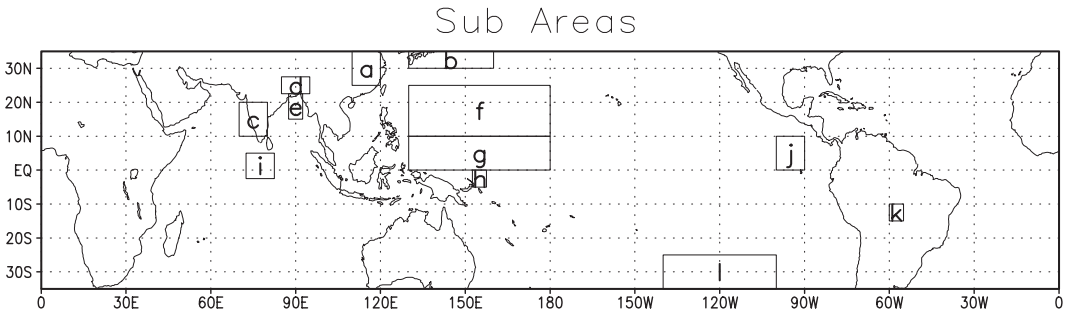

FIG. 14. Map of subdomains shown in Figs. 15 and 16. Letters shown in each box indicate the name of the corresponding domain.

This finding is consistent with previous cloud physical predictions that low-number densities of CCN over ocean are favorable for generating warm rain (Beard and Ochs 1984, 1993). Our results show a strong positive correlation between warm rain and SST. The relationship is significant in both the tropics and the subtropics, whereas the positive correlation between total rain and SST is confined to the tropics. Warm rain is scarce over oceans with low-level cloudiness greater than 40%. Strong warm rain is observed when low-level cloudiness is around 20%–30%. This result is consistent with previous findings that strong warm rain is provided not by stratiform clouds but by convective clouds, which are favorable for coalescence processes. We conclude that warm rain is associated with oceans, especially warm oceans.

The significant positive correlation between SST and warm rain is a new finding of this study that suggests that warm rain is strongly influenced by some process in the maritime boundary layer controlled by SST. Johnson et al. (1999) showed that the number of congestus clouds increased with increasing SST in the TOGA COARE area. Our results extend such relationships to most portions of the tropical and subtropical oceans. Further studies are needed, especially on boundary layer processes influenced by SST, which may be related to boundary layer clouds and cumulus congestus. Cloud physical processes are also candidates to explain the linkage. Lau and Wu (2003) demonstrated that the autoconversion process for light warm rain is activated by an increase of SST. SST may also be related to the activation and number concentration of CCN; for example, relationships exist between sea salt CCN and wet conditions in the subcloud layer (Woodcock 1953) and between lower SST and the generation of CCN from dimethyl sulfide (Hegg et al. 1991).

Our second finding is the large contribution of warm rain to LH in the marine atmospheric boundary layer. Despite its small contribution to total rain over oceans (5%–20%), warm rain maintains positive LH over most of the tropical and subtropical oceans. LH from warm rain masked low-level cooling by stratiform rain and maintained positive LH in the lower atmosphere below the ML. Because warm rain is confined to the ocean, a strong low-level LH contrast is maintained along the coast. In the tropics, the LH contrast is greater in summer when negative LH is intensified over land. The LH contrast reaches 1–2 K day^{-1} in places and may affect local and monsoonal circulation across the continental coasts.

To confirm these results, we must evaluate the accuracy of shallow rain observations by TRMM PR, as noted by Short and Nakamura (2000) and Cifelli et al. (2007). In the PRH algorithm, downward attenuation of radar reflectivity is considered to be evaporation of precipitation, that is, negative LH (Satoh 2004; Tao et al. 2006). We found strong negative LH in the atmospheric boundary layer over land. This seems reasonable, considering the dry condition of the ABL over land, which is favorable for negative LH. Low-level latent cooling over land is also maintained by the lack of LH by warm rain, which is weak over land. However, we need to examine the quantitative reliability of warm rain intensity and accompanying LH over land. Small-sized shallow rain may be dominant over land, rather than over the oceans. Small cloud size comparable to or less than the instantaneous field of view (IFOV) of TRMM PR (4.3 km originally and 5.0 km MSL after the reboost of TRMM in 2001) may cause weak bias in rainfall intensity by partial beam filling. Moreover, missed observations of weak rainfall under the detectable level of the PR (18 dBZ) would also cause weak bias, if weaker rainfall were more dominant over land. The underestimation of shallow rain in PR observations over land causes the overestimation of latent cooling over land and the land–ocean LH contrast in the lower troposphere. The results of our study on LH profiles depend on the TRMM PR observations and the version 6.4 PRH algorithm. Further studies, especially observational studies of warm rain, are necessary to examine the reliability of LH estimated by the PRH algorithms.

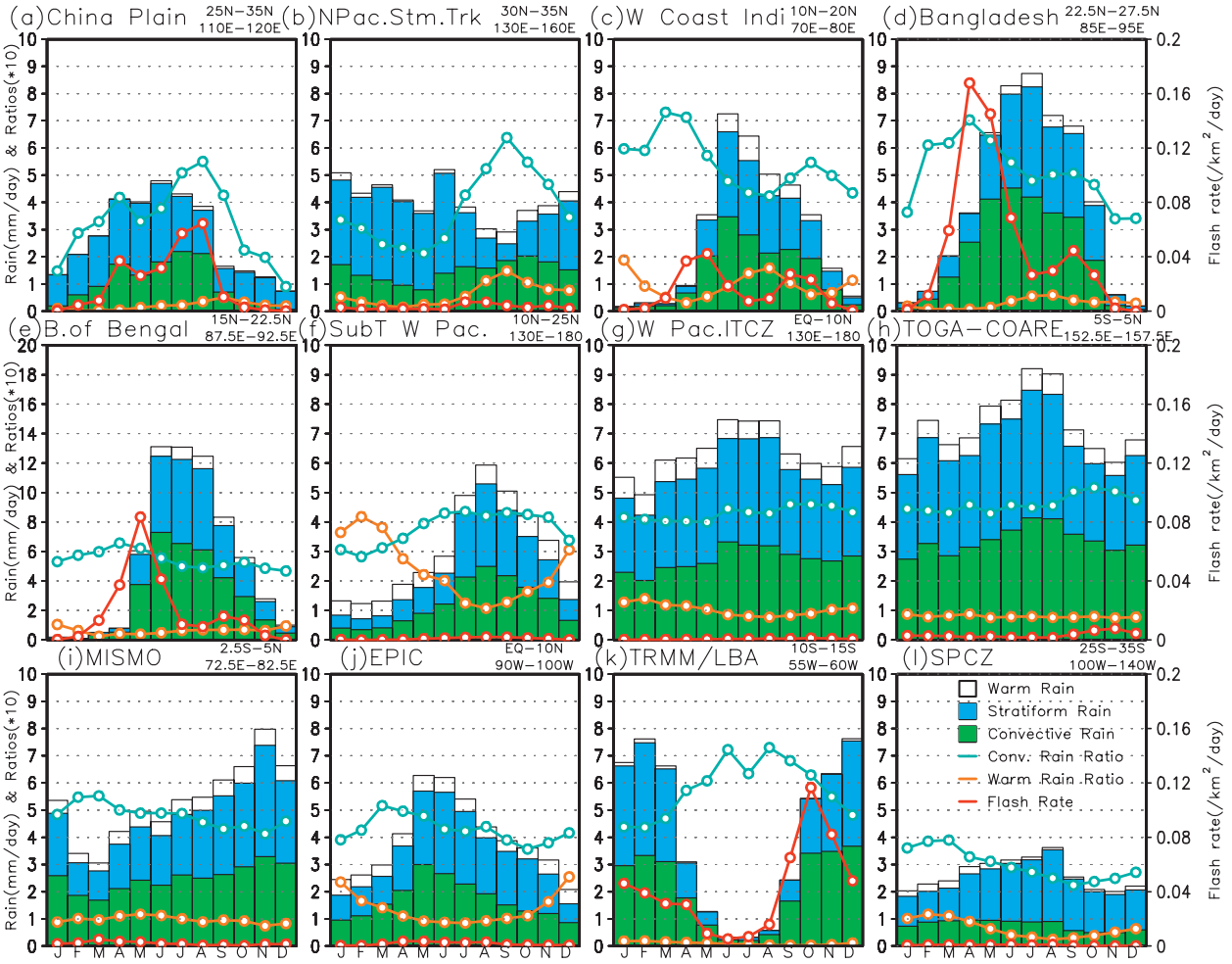

FIG. 15. Same as in Fig. 7 but for the selected subdomains adopted in Fig. 14: the (a) China plain, (b) storm track over the North Pacific, (c) west coast of India, (d) Bangladesh, (e) Bay of Bengal, (f) western North Pacific in the subtropics, (g) ITCZ in the western Pacific, (h) TOGA COARE field in the western equatorial Pacific, (i) MISMO field in the tropical Indian Ocean, (j) EPIC field in the ITCZ over the eastern Pacific, (k) TRMM-LBA field over the Amazon basin, and (l) SPCZ.

Our third finding is that the relationship between warm rain and total rain differs between the ITCZ and STCZs. Strong warm rain is observed in the ITCZ. Warm rain is also rather strong in tropical monsoon rainfall over oceans (i.e., the warm water pools over the western Pacific and eastern Indian oceans). This is also consistent with the findings of Johnson et al. (1999). However, warm rain is weak in the subtropical portion of the STCZs. This may be ascribed to lower SST in these zones because fairly strong warm rain coexists in the upstream of low-level flow toward the STCZ along the periphery of subtropical highs, where SST is higher. Johnson et al. (1996) suggested that inversion of the 0°C level, which may cause cumulus congestus, can form from the negative LH of the snow melting process, which is provided by deep convections. Subtropical portions of STCZs are also characterized by active deep convections (Kodama 1992). We need to investigate the stratification in the STCZs to examine the existence of a stable layer near the ML and the instability maintaining shallow convections and congestus clouds in the lower troposphere.

Acknowledgments. This study was financially supported as a cooperative study between the Japan Aerospace Exploration Agency (JAXA) and Hirosaki University and also partially supported by a Grant-in-Aid for Scientific Research (19403009) of the Japanese Ministry of Education, Science, and Culture, supervised by Prof. Tsuda. TRMM data were provided by the JAXA Earth Observation Research Center and the Goddard Space Flight Center/Distributed Active Archive Center. We used SST and OLR data provided by NOAA, ISCCP-D2 cloudiness data provided by NASA Goddard Institute for Space Studies, and National Centers for Environmental

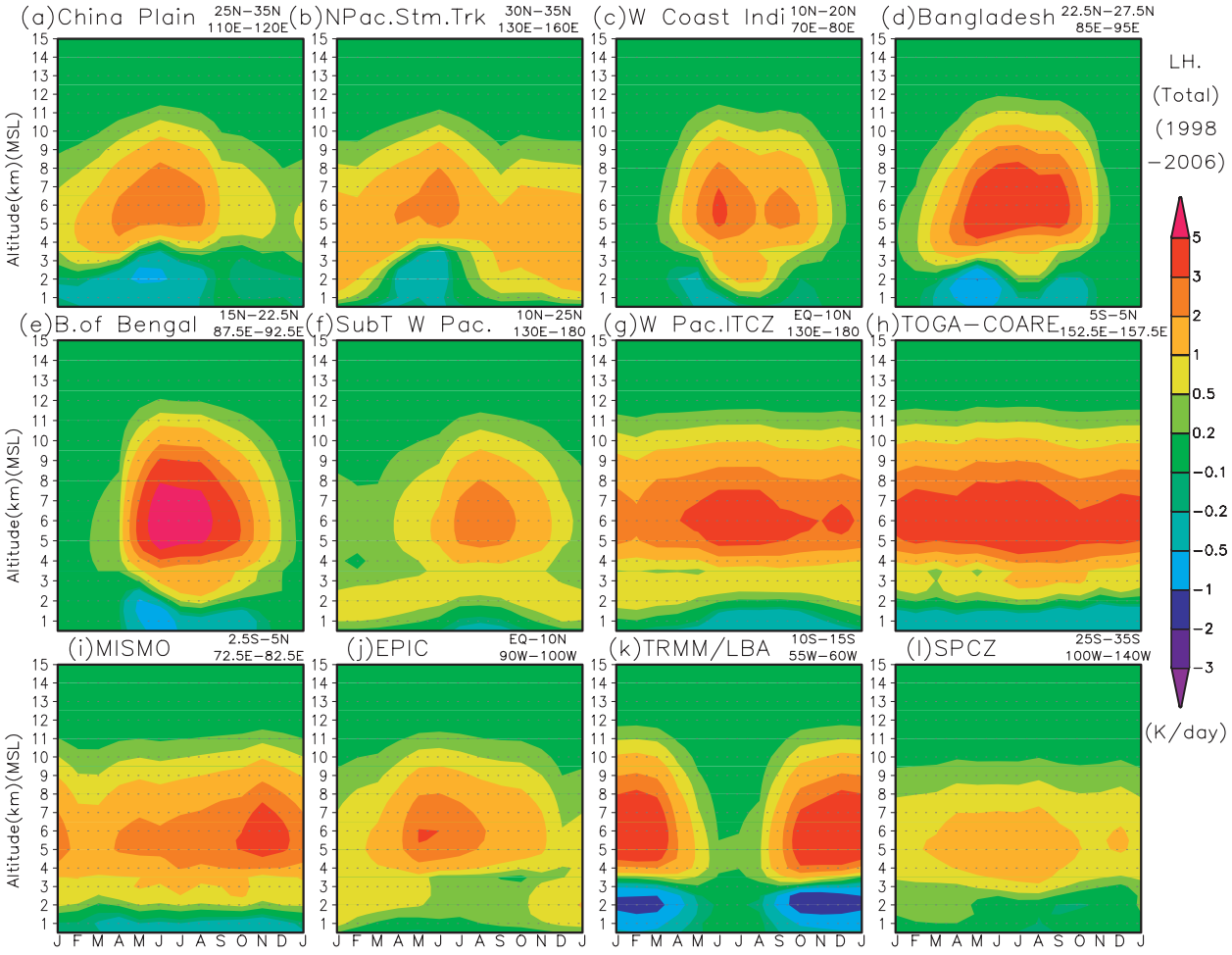

FIG. 16. Same as in Fig. 11 but for the selected subdomains adopted in Fig. 14.

Prediction–National Center for Atmospheric Research (NCEP–NCAR) reanalysis data provided by NOAA/ Earth System Research Laboratory. We appreciate Prof. A. D. Del Genio and three anonymous reviewers for providing very constructive comments.

APPENDIX

PRH Algorithm

In this study, we use an improved version (version 6.4) of the PRH algorithm proposed by Katsumata (2007), which originated from the algorithm developed by Satoh and Noda (2001) and Satoh (2004). The PRH algorithm is a variation of the thermodynamic retrieval from the radar data (Roux and Sun 1990), which uses a vertical profile of the radar reflectivity obtained by TRMM PR. The PRH algorithm enables us to retrieve LH over variable geographical conditions with high vertical resolution. The low sensitivity of TRMM PR observation (lower limit of ~18 dBZ) for ice-phase precipitation may cause the underestimation of LH above the ML, whereas the estimation of LH below the ML seems to be more reliable.

In the PRH algorithm, the sign of LH is assumed to depend on the sign of productivity of the precipitation mixing ratio, which is evaluated from the vertical gradient of the precipitation mixing ratio observed by PR, vertical wind speed, and terminal velocity of precipitation. Negative productivity results in negative LH to reflect the evaporation cooling of precipitation particles. Positive productivity results in positive LH to reflect the condensation. Negative LH is evaluated from the productivity of the precipitation, whereas the positive LH is evaluated from the condensation rate derived from the vertical wind and vertical profile of the saturated mixing ratio. This is because the cloud droplet, which is formed by the condensation, cannot be detected by TRMM PR.

The vertical wind profiles are approximated as the fourth-order polynomial function between ground surface and the tropopause. The height of the nodes, in which the value is zero, is determined for four rain types: convective, stratiform, shallow, and anvil. The rain type is determined for each ray of TRMM PR observations following Table 1 using indexes of precipitation in the version 6 TRMM PR 2A25 product. In the convective and shallow rays, the cloud base and the cloud top are determined as nodes to give the updraft within the layer between them. In the stratiform and anvil rays, the nodes are determined at around the ML and cloud top to give the updraft between them and downdraft below around the ML. The vertical extent and node heights of vertical wind profiles are obtained from the echo-top height and melting-layer height, which is given from the TRMM PR 2A25 product. The functions to estimate node heights were determined statistically by using the dataset from the Equatorial Atmospheric Radar, a large very high-frequency (VHF) radar, in Sumatra, Indonesia (Fukao 2006; Mori et al. 2006), and dual-Doppler observations at the Palau Islands, in the western Pacific (Moteki et al. 2007). Finally, the amplitude of the vertical wind profiles described by polynomial functions is determined iteratively to match the estimated LH, in the unit of rain rate, to the observed rain rate at ground (actually using near-surface rain) and at the node near the ML.

REFERENCES

Beard, K. V., and H. T. Ochs III, 1984: Collection and coalescence efficiencies for accretion. *J. Geophys. Res.,* **89** (D5), 7165–7169.

——, and ——, 1993: Warm-rain initiation: An overview of microphysical mechanisms. *J. Appl. Meteor.,* **32,** 608–625.

Cecil, D. J., S. J. Goodman, D. J. Boccippio, E. J. Zipser, and S. W. Nesbitt, 2005: Three years of TRMM precipitation features. Part I: Radar, radiometric, and lightning characteristics. *Mon. Wea. Rev.,* **133,** 543–566.

Cifelli, R., S. W. Nesbitt, A. Rutledge, W. A. Petersen, and S. Yuter, 2007: Radar characteristics of precipitation features in the EPIC and TEPPS regions of the east Pacific. *Mon. Wea. Rev.,* **135,** 1576–1595.

DeMoss, J. D., and K. P. Bowman, 2007: Changes in TRMM rainfall due to the orbit boost estimated from buoy rain gauge data. *J. Atmos. Oceanic Technol.,* **24,** 1598–1607.

Fukao, S., 2006: Coupling processes in the equatorial atmosphere (CPEA): A project overview. *J. Meteor. Soc. Japan,* **84A,** 1–18.

Hegg, D. A., L. F. Radke, and P. V. Hobbs, 1991: Measurements of Aitken nuclei and cloud condensation nuclei in the marine atmosphere and their relation to the DMS-cloud-climate hypothesis. *J. Geophys. Res.,* **96** (D10), 18 727–18 733.

Houze, R. A., Jr., 1993: *Cloud Dynamics.* Academic Press, 573 pp.

Johnson, R. H., P. E. Ciesielski, and K. A. Hart, 1996: Tropical inversions near the 0°C level. *J. Atmos. Sci.,* **53,** 1838–1855.

——, T. M. Rickenbach, S. A. Rutledge, P. E. Ciesielski, and W. H. Schubert, 1999: Trimodal characteristics of tropical convection. *J. Climate,* **12,** 2397–2418.

Katsumata, M., 2007: Study on the structure of the precipitating systems related to the latent heating profiles (in Japanese). TRMM research report, T. Nakazawa, Ed., JAXA/EORC, 197–223.

Kiguchi, M., and J. Matsumoto, 2005: The rainfall phenomena during the pre-monsoon period over the Indochina peninsula in the GAME-IOP year, 1998. *J. Meteor. Soc. Japan,* **83,** 89–106.

Klett, J. D., and M. H. Davis, 1973: Theoretical collision efficiencies of cloud droplets at small Reynolds numbers. *J. Atmos. Sci.,* **30,** 107–117.

Kodama, Y.-M., 1992: Large-scale common features of subtropical precipitation zones (the Baiu frontal zone, the SPCZ, and the SACZ) Part I: Characteristics of subtropical frontal zones. *J. Meteor. Soc. Japan,* **70,** 813–836.

——, 1993: Large-scale common features of subtropical convergence zones (the Baiu frontal zone, the SPCZ, and the SACZ) Part II: Conditions of the circulations for generating the STCZs. *J. Meteor. Soc. Japan,* **71,** 581–610.

——, and A. Tamaoki, 2002: A re-examination of precipitation activity in the subtropics and the mid-latitudes based on satellite-derived precipitation data. *J. Meteor. Soc. Japan,* **80,** 1261–1278.

——, A. Ohta, M. Katsumata, S. Mori, S. Satoh, and H. Ueda, 2005: Seasonal transition of predominant precipitation type and lightning activity over tropical monsoon areas derived from TRMM observations. *Geophys. Res. Lett.,* **32,** L14710, doi:10.1029/2005GL022986.

——, H. Okabe, Y. Tomisaka, K. Kotono, Y. Kondo, and H. Kasuya, 2007: Lightning frequency and microphysical properties of precipitating clouds over the western North Pacific during winter as derived from TRMM multisensor observations. *Mon. Wea. Rev.,* **135,** 2226–2241.

Lau, K.-M., and H.-T. Wu, 2003: Warm rain processes over tropical oceans and climate implications. *Geophys. Res. Lett.,* **30,** 2290, doi:10.1029/2003GL018567.

——, ——, and S. Bony, 1997: The role of large-scale atmospheric circulation in the relationship between tropical convection and sea surface temperature. *J. Climate,* **10,** 381–392.

Liebmann, B., and C. A. Smith, 1996: Description of a complete (interpolated) outgoing longwave radiation dataset. *Bull. Amer. Meteor. Soc.,* **77,** 1275–1277.

Lin, X., and R. H. Johnson, 1996: Heating, moistening, and rainfall over the western Pacific warm pool during TOGA COARE. *J. Atmos. Sci.,* **53,** 3367–3383.

Luo, H., and M. Yanai, 1984: The large-scale circulation and heat sources over the Tibetan plateau and surrounding areas during the early summer of 1979. Part II: Heat and moisture budgets. *Mon. Wea. Rev.,* **112,** 966–989.

Masunaga, H., T. S. L'Ecuyer, and C. D. Kummerow, 2005: Variability in the characteristics of precipitation systems in the tropical Pacific. Part I: Spatial structure. *J. Climate,* **18,** 823–840.

Mori, S., and Coauthors, 2006: Vertical wind characteristics in precipitating cloud systems over West Sumatera, Indonesia, by the equatorial atmospheric radar: Case study of 23–24 April 2004 during the first CPEA campaign period. *J. Meteor. Soc. Japan,* **84A,** 95–112.

Moteki, Q., and Coauthors, 2007: The impact of the assimilation of dropsonde observations during PALAU2005 in ALERA. *SOLA,* **3,** 97–100, doi:10.2151/sola.2007-025.

Murakami, T., L.-X. Chen, and A. Xie, 1986: Relationship among seasonal cycles, low-frequency oscillations, and transient

disturbances as revealed from outgoing longwave radiation data. *Mon. Wea. Rev.,* **114,** 1456–1465.

Nakazawa, T., and K. Rajendran, 2009: Interannual variability of tropical rainfall characteristics and the impact of the altitude boost from TRMM PR 3A25 data. *J. Meteor. Soc. Japan,* **87A,** 317–338.

Neggers, R. A., J. D. Neelin, and B. Stevens, 2007: Impact mechanisms of shallow cumulus convection on tropical climate dynamics. *J. Climate,* **20,** 2623–2642.

Nigam, S., C. Chung, and E. DeWeaver, 2000: ENSO diabatic heating in ECMWF and NCEP–NCAR reanalyses, and NCAR CCM3 simulation. *J. Climate,* **13,** 3152–3171.

Ninomiya, K., 1984: Characteristics of Baiu front as predominant subtropical front in the summer Northern Hemisphere. *J. Meteor. Soc. Japan,* **62,** 880–892.

——, 2007: Similarity and difference between the South Atlantic convergence zone and the Baiu frontal zone simulated by an AGCM. *J. Meteor. Soc. Japan,* **85,** 277–299.

——, 2008: Similarities and differences among the South Indian Ocean convergence zone, the North American convergence zone, and other subtropical convergence zones simulated by an AGCM. *J. Meteor. Soc. Japan,* **86,** 141–165.

Ogura, Y., and T. Takahashi, 1973: The development of warm rain in a cumulus model. *J. Atmos. Sci.,* **30,** 262–277.

Pereira, L. G., and S. A. Rutledge, 2006: Diurnal cycle of shallow and deep convection for a tropical land and an ocean environment and its relationship to synoptic wind regimes. *Mon. Wea. Rev.,* **134,** 2688–2701.

Petersen, W. A., and S. A. Rutledge, 2001: Regional variability in tropical convection: Observations from TRMM. *J. Climate,* **14,** 3566–3586.

Raymond, D. J., and Coauthors, 2004: EPIC2001 and the coupled ocean–atmosphere system of the tropical east Pacific. *Bull. Amer. Meteor. Soc.,* **85,** 1341–1354.

Reynolds, R. W., N. A. Rayner, T. M. Smith, D. C. Stokes, and W. Wang, 2002: An improved in situ and satellite SST analysis for climate. *J. Climate,* **15,** 1609–1625.

Rogers, R. R., and M. K. Yau, 1989: *A Short Course in Cloud Physics*. 3rd ed. Pergamon Press, 121–149.

Rossow, W. B., and R. A. Schiffer, 1999: Advances in understanding clouds from ISCCP. *Bull. Amer. Meteor. Soc.,* **80,** 2261–2287.

Roux, F., and S. Ju, 1990: Single-Doppler observations of a West African squall line on 27-28 May 1981 during COPT81: Kinematics, thermodynamics and water budget. *Mon. Wea. Rev.,* **118,** 1826–1854.

Satoh, S., 2004: Retrieval of latent heating profiles in various cloud systems from TRMM radar data. Report on the latent heating algorithms developed for TRMM PR data, T. Nakazawa, Ed., JAXA/EORC, 57–76.

——, and A. Noda, 2001: Retrieval of latent heating profiles from TRMM radar data. Preprints, *30th Int. Conf. on Radar Meteorology,* Munich, Germany, Amer. Meteor. Soc., 6.3. [Available online at http://ams.confex.com/ams/30radar/techprogram/paper_21763.htm.]

Schiffer, R. A., and W. B. Rossow, 1983: The International Satellite Cloud Climatology Project (ISCCP): The first project of the World Climate Research Programme. *Bull. Amer. Meteor. Soc.,* **64,** 779–784.

Schumacher, C., M. H. Zhang, and P. E. Ciesielski, 2007: Heating structure of the TRMM field campaigns. *J. Atmos. Sci.,* **64,** 2593–2610.

Shige, S., Y. N. Takayabu, W.-K. Tao, and D. E. Johnson, 2004: Spectral retrieval of latent heating profiles from TRMM PR data. Part I: Development of a model-based algorithm. *J. Appl. Meteor.,* **43,** 1095–1113.

——, ——, ——, and C.-L. Shie, 2007: Spectral retrieval of latent heating profiles from TRMM PR data. Part II: Algorithm improvement and heating estimates over tropical ocean regions. *J. Appl. Meteor. Climatol.,* **46,** 1098–1124.

Shinoda, T., H. Uyeda, and K. Yoshimura, 2005: Structure of moist layer and sources water over the southern region far from the Meiyu/Baiu front. *J. Meteor. Soc. Japan,* **83,** 137–152.

Short, D. A., and K. Nakamura, 2000: TRMM radar observation of shallow precipitations over the tropical oceans. *J. Climate,* **13,** 4107–4124.

Silva Dias, M. A. F., and Coauthors, 2002: Cloud and rain processes in a biosphere-atmosphere interaction context in the Amazon Region. *J. Geophys. Res.,* **107,** 8072, doi:10.1029/2001JD000335.

Simpson, J., R. F. Adler, and G. R. North, 1988: A proposed Tropical Rainfall Measuring Mission (TRMM) satellite. *Bull. Amer. Meteor. Soc.,* **69,** 278–295.

Stevens, B., W. R. Cotton, G. Feingold, and C.-H. Moeng, 1998: Large-eddy simulations of strongly precipitating, shallow, stratocumulus-topped boundary layers. *J. Atmos. Sci.,* **55,** 3616–3638.

Takahashi, T., 1981: Warm rain development in a three-dimensional cloud model. *J. Atmos. Sci.,* **38,** 1991–2003.

Tao, W.-K., and Coauthors, 2006: Retrieval of latent heating from TRMM measurements. *Bull. Amer. Meteor. Soc.,* **87,** 1555–1572.

Thompson, R. M., Jr., S. W. Payne, E. E. Recker, and R. J. Reed, 1979: Structure and properties of synoptic-scale wave disturbances in the intertropical convergence zone of the eastern Atlantic. *J. Atmos. Sci.,* **36,** 53–72.

Trewartha, G. T., and L. H. Horn, 1980: *An Introduction to Climate*. McGraw-Hill, 416 pp.

TRMM Precipitation Radar Team, 2005: Tropical Rainfall Measuring Mission (TRMM) Precipitation Radar Algorithm instruction manual for version 6. Japan Aerospace Exploration Agency and NASA Rep., 180 pp. [Available online at http://www.eorc.jaxa.jp/TRMM/documents/PR_algorithm_product_information/pr_manual/pr_manual_v6.pdf.]

Ueda, H., H. Kamahori, and N. Yamazaki, 2003: Seasonal contrasting features of heat and moisture budgets between the eastern and western Tibetan Plateau during the GAME IOP. *J. Climate,* **16,** 2309–2324.

Webster, P. J., and R. Lukas, 1992: TOGA COARE: The coupled ocean–atmosphere response experiment. *Bull. Amer. Meteor. Soc.,* **73,** 1377–1416.

Woodcock, A. H., 1953: Salt nuclei in marine air as a function of altitude and wind force. *J. Meteor.,* **10,** 362–371.

Xie, S.-P., H. Xu, N. H. Saji, and Y. Wang, 2006: Roles of narrow mountains in large-scale organization of Asian monsoon convection. *J. Climate,* **19,** 3420–3429.

Yanai, M., and M. Tomita, 1998: Seasonal and interannual variability of atmospheric heat sources and moisture sinks as determined from NCEP–NCAR reanalysis. *J. Climate,* **11,** 463–482.

——, S. Esbensen, and J.-H. Chu, 1973: Determination of bulk properties of tropical cloud clusters from large-scale heat and moisture budgets. *J. Atmos. Sci.,* **30,** 611–627.

Yoneyama, K. Y., and Coauthors, 2008: MISMO field experiment in the equatorial Indian Ocean. *Bull. Amer. Meteor. Soc.,* **89,** 1889–1903.

Zhang, C., 1993: Large-scale variability of atmospheric deep convection in relation to sea surface temperature in the tropics. *J. Climate,* **6,** 1898–1913.